NASA CONTRACTOR REPORT

NASA CR-2153

NASA CR-2153

CORRELATION TECHNIQUES AND MEASUREMENTS OF WAVE-HEIGHT STATISTICS

by H. Guthart, W. C. Taylor, K. A. Graf, and D. G. Douglas

Prepared by
STANFORD RESEARCH INSTITUTE
Menlo Park, Calif. 94025
for Langley Research Center

NATIONAL AERONAUTICS AND SPACE ADMINISTRATION • WASHINGTON, D. C. • DECEMBER 1972

1. Report No.	2. Government Accession No.	3. Recipient's Catalog No.
NASA CR-2153		

4. Title and Subtitle	5. Report Date
CORRELATION TECHNIQUES AND MEASUREMENTS OF WAVE-HEIGHT STATISTICS	December 1972
	6. Performing Organization Code

7. Author(s)	8. Performing Organization Report No.
H. Guthart W. C. Taylor K. A. Graf D. G. Douglas	SRI Project 1183

9. Performing Organization Name and Address	10. Work Unit No.
Stanford Research Institute Menlo Park, California 94025	11. Contract or Grant No. NAS1-10681

12. Sponsoring Agency Name and Address	13. Type of Report and Period Covered
National Aeronautics and Space Administration Washington, D.C. 20546	Contractor Report
	14. Sponsoring Agency Code

15. Supplementary Notes

16. Abstract

Statistical measurements of wave-height fluctuations have been made in a wind-wave tank. The power spectral density function of temporal wave-height fluctuations evidenced second-harmonic components and an f^{-5} power-law decay beyond the second harmonic. The observations of second-harmonic effects agreed very well with a theoretical prediction. From the wave statistics, surface drift currents were inferred and compared to experimental measurements with satisfactory agreement. Measurements were made of the two dimensional correlation coefficient at 15° increments in angle with respect to the wind vector. An estimate of the two-dimensional spatial power spectral density function was also made.

17. Key Words	18. Distribution Statement
surface waves; correlation coefficient; power spectral density function; second harmonics; drift currents	

19. Security Classif. (of this report)	20. Security Classif. (of this page)	21. No. of Pages	22. Price*
Unclassified	Unclassified	52	$3.00

* For sale by the National Technical Information Service, Springfield, Virginia 22151

CONTENTS

ILLUSTRATIONS

CORRELATION TECHNIQUES AND MEASUREMENTS OF WAVE-HEIGHT STATISTICS

H. Guthart W. C. Taylor K. A. Graf D. G. Douglas
Stanford Research Institute
Menlo Park, California 94025

I INTRODUCTION

Electromagnetic interactions with the sea have been the subject of some study for a number of years.[1]* These studies, however, have been severely hampered by an incomplete description of the scattering surface.[2] As a consequence, a verification of theoretical models has been difficult to obtain. While an assessment of different scatter models could require measurements of various different characteristics of the surface, the most useful description of the surface is probably the correlations of the wave heights. The two-dimensional spatial correlation of the surface heights, $R(\vec{\delta})$, is given by:

$$R(\vec{\delta}) = \frac{\overline{\tilde{h}(\vec{r}_1)\ \tilde{h}(\vec{r}_1 + \vec{\delta})}}{h'(\vec{r}_1)\ h'(\vec{r}_1 + \vec{\delta})} \qquad \text{(1a)}$$

where $\tilde{h}$ is the fluctuating component of wave height, $\vec{\delta}$ is the separation between sensing points, the overbar designates a spatial average, and h' is the root-mean-square value of the fluctuating component of wave height. The spatial correlation coefficient, $R(\vec{\delta})$, is the two-dimensional Fourier transform of the power spectral density frunction of the surface fluctuations. In general, the spatial correlation is expected to be anisotropic. In addition to the spatial correlation coefficient, the type of measurements that could be expected to specify the scattered electromagnetic signal would include space-time correlations, $R(\vec{\delta},\tau)$,

* References are listed at the end of the report.

$$R(\vec{\delta},\tau) = \frac{\overline{\tilde{h}(\vec{r},t)\,\tilde{h}(\vec{r}+\vec{\delta},\,t+\tau)}}{h'(\vec{r})\,h'(\vec{r}+\vec{\delta})}\,, \qquad (1b)$$

where τ is the time lag. Such measurements should be capable of predicting not only the mean level of the reflected signal, but also the statistical nature of the scattered electromagnetic signal.

For small wave heights ($h \ll \lambda$) the electromagnetic scattering from the surface is considered to be proportional to the power spectral density (PSD) of the wave-height fluctuations (i.e., the interaction is described by Bragg scattering). As a consequence, a backscatter radar measures the surface fluctuations at a discrete wavelength--namely, $(\lambda/2 \sin \theta)$, where λ is the radar wavelength and θ is the angle of incidence with the zenith. A verification of the model for the scattering of electromagnetic waves from the sea surface, then, requires a measurement of wave statistics at a wavelength of $(\lambda/2 \sin \theta)$. Unfortunately, early radar experiments did not have the accompanying "sea truth" measurements and the results are surrounded by considerable controversy,

Radar (or radiometric) measurements are usually made in the centimeter-wavelength band, corresponding to the short-gravity-wave and capillary-wave portion of the spectrum. Recent results reported by Pierson[3] indicate that the capillary-wave part of the spectrum does not "saturate." This is a very important result, for it indicates that an estimate of the capillary-wave spectrum cannot be inferred from the gravity-wave spectrum. In addition, the capillary-wave spectrum is most sensitive to local wind conditions and therefore subject to a good deal of variability. These considerations indicate the need and desirability for short-gravity-wave and capillary-wave measurements if the questions and controversy surrounding the electromagnetic interactions with the sea are to be resolved.

In the past, several means have been used for measuring the surface fluctuations. These are (1) resistance-type or capacitance-type wave-height gauges, (2) optical sensors, and (3) accelerometers. These three alternative techniques offer significantly different measurements of the surface fluctuations. The accelerometer size suggests its unsuitability for measurement of wave-height statistics in the centimeter-wavelength regime. Optical and wave-staff techniques will be discussed in Section II, including the development of the resistance-type staff used in these studies.

Section III describes the initial measurement of wave-height correlations actually undertaken in the SRI wind-wave tank.

Section IV discusses the results of the wave-height measurements described in Section III.

The conclusions of these studies are discussed in Section V, where recommendations for future studies are also put forward.

It is a pleasure to acknowledge Prof. H. Medwin of the Naval Post-graduate School and Prof. E. Y. Hsu of Stanford University for their generous assistance in setting up the experiment.

The authors are further indebted to G. R. Hilbers, J. W. Granville, and R. L. Martin of the Electromagnetic Sciences Laboratory, SRI for their invaluable assistance in the performance of these tests.

II WAVE-HEIGHT-SENSOR DEVELOPMENT

In this section, some of the alternative schemes for optical sensing of wave-height fluctuations will be briefly surveyed. This discussion will be followed by an analysis of the resistance-type wave staffs used in these experiments. The first two optical methods described can, in principle, provide instantaneous spatial measurements of the surface. The laser profilometer and the wave staffs described in the next section make "point" measurements, and ergodicity must be assumed to relate such measurements to spatial statistics. The assumption about ergodicity is easily justified but the stationarity of surface conditions during the time required to make temporal measurements can impose a requirement for an array of point sensors.

A. Optical Sensors

Optical sensing of wave-height fluctuations has the promise of measurements without perturbation of the wave medium. As a consequence, a good deal of effort is going into the development of optical means for sensing wave-height fluctuations. The earliest optical techniques recorded the light reflections from the surface to determine the probability density function of wave slopes. This is accomplished by taking advantage of the specular nature of the scattering of light rays from a surface. For a given geometry, light will be scattered into a detector only when the normal wave slope is collinear with the bisector to the angle formed by the illuminator, the surface, and the detector. By measuring the percentage of the time that glints occur for a given scatter geometry (and therefore, for a specified wave slope), the probability density function is determined. The light source for the early measurements was a flash bulb[4] and the sun[5]. The detector was film. These experiments have two drawbacks from the point of view of

of the goals of this program. In the first place, the photographic method utilized involved tedious and slow data analysis. This constraint has been circumvented by Wu et al.[6], and their techniques can be improved still further with laser illumination and correlation tube detection. The second drawback of this system is that the probability density function of the slopes cannot be related to the PSD function of wave heights. It is therefore unrelated to the electromagnetic backscatter at microwave frequencies. "Glints" occur only when slopes are very near specular, so such a system has almost no dynamic range for slope measurements. Stilwell[7] developed a system for measurement of the PSD of the wave-slope fluctuations. This quantity is k^2 (where k is the wavenumber) times the PSD of the wave-height fluctuations and is indeed pertinent for comparison with electromagnetic scatter measurements. In this technique, the sky brightness is taken as a uniform illuminator, or at least a known monotonic illuminator, of the sea surface. The light reaching a point at the observer is then a Fourier transform of the wave-slope distribution, for every point on the surface has a ray incident with the proper orientation for specular scatter to the observing point. The technique as pioneered by Stilwell requires considerable data processing of the photographic plates. Also, the background illumination must remain constant (and uniform), or it must be monitored.

A third optical technique for wave-height sensing is the laser profilometer. In this technique a laser is modulated with an RF wave and used to illuminate a spot on the sea surface. The reflected signal is detected and the phase of the modulating signal is measured. The phase history of the reflected signal is then a measure of the wave-height fluctuations. The initial utilization of this technique[8] involved helium-neon lasers operating at 632.8 nanometers. The large skin depths (2 m in salt water) preclude the measurement of small gravity and

capillary waves. SRI is currently working on a program for the Advanced Research Projects Agency to adapt this technique to the infrared portion of the spectrum (wavelength = 10.6 μ), where the skin depths are very small ($\sim$ 10 μ). This technique also has the very desirable property that the data outputs are computer-compatible.

There are optical refraction methods[9] for wave-height sensing; however, such schemes would involve the submergence of components if if the method were to be used on the open sea. With submerged components, this technique becomes less attractive in non-laboratory experiments, since it throws away one of the principal advantages of optical wave-height sensing--i.e., the capability of a non-contacting sensor.

B. Wave Staffs

Wave staffs have classically been operated as resistance or capacitive devices. The systems have the obvious advantage of being inexpensive, and conceptually and electronically simple. Also, their outputs are computer-compatible. The greatest uncertainty regarding these probes concerns the effect of meniscus on the probes. Indeed, there have been reports of distortion[10] on capacitive wave staffs. The distortion is reported to occur at frequencies above 20 Hz and is thought to be a consequence of probe wetting. The same study indicates that resistance-type staffs are distortion-free.

As an outgrowth of the foregoing, resistance-type wave staffs have been chosen for wave-height sensing in this program. Resistance-type staffs have two configurations. For fresh water, low-resistance wires are used, giving essentially zero wire resistance, and the resistance of the water is measured as a function of probe depth. For salt water (with its much

higher conductivity), high-resistance wires are used; the water acts as a short circuit for the wire and the measured resistance is proportional to the length of probe not in the water.

C. Development of a Resistance-Type Wave Staff

The development of a resistance-type wave staff was undertaken for initial application to a fresh-water wind-wave tank. The geometry of the probe is shown in Figure 1. The sensing wire has a diameter of 0.16 cm. The circuit is completed with a ground wire that is sheathed so that the part in contact with water is independent of wave height. The spatial resolution of such a wave staff is then specified by the diameter of the sensing electrode, independent of the interelectrode spacing.

Electrolytic effects dictated the choice of an alternating-current probe (in contrast to a dc probe). Since measurements of wave-height fluctuations occur at frequencies of the order of tens of Hertz, an alternating frequency to remove electrolytic effects was selected in the kilohertz regime to obtain the desired separation between the carrier frequency and the wave frequencies to be measured.

Since the goal of these experiments is to measure the spatial correlation coefficient of the wave-height fluctuations, a pair of wave staffs was designed. To minimize the coupling between staffs, the probes were operated at two frequencies unharmonically related (175 kHz and 280 kHz). A block diagram of the electronic systems is shown in Figure 2. The probe common-mode filters, shown in Figure 2, were designed to minimize the coupling between staffs. The bridge of Figure 2 is used to cancel the bias voltage around the operating point of the probe, so that the fluctuations in voltage produced by the wave-height fluctuations can be amplified without overloading the detector. A calibration for this

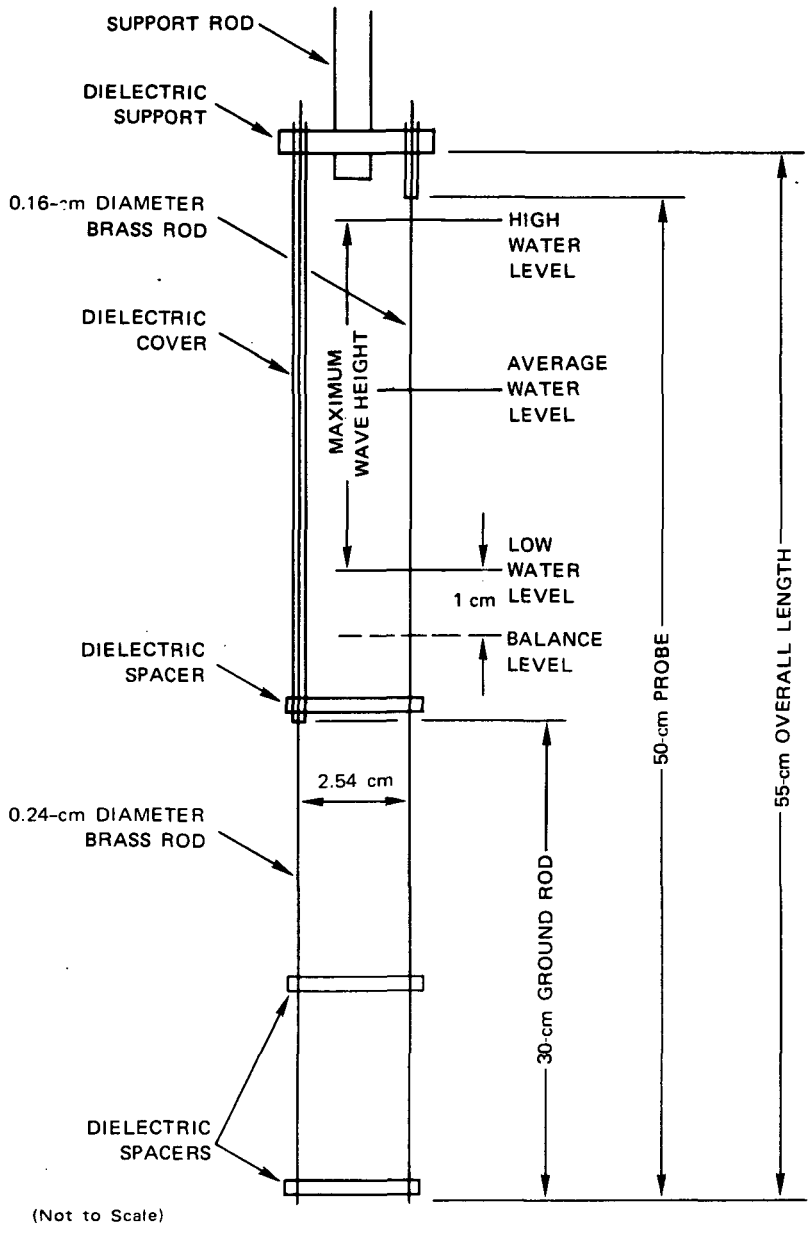

FIGURE 1 NOMINAL PROBE CONFIGURATION

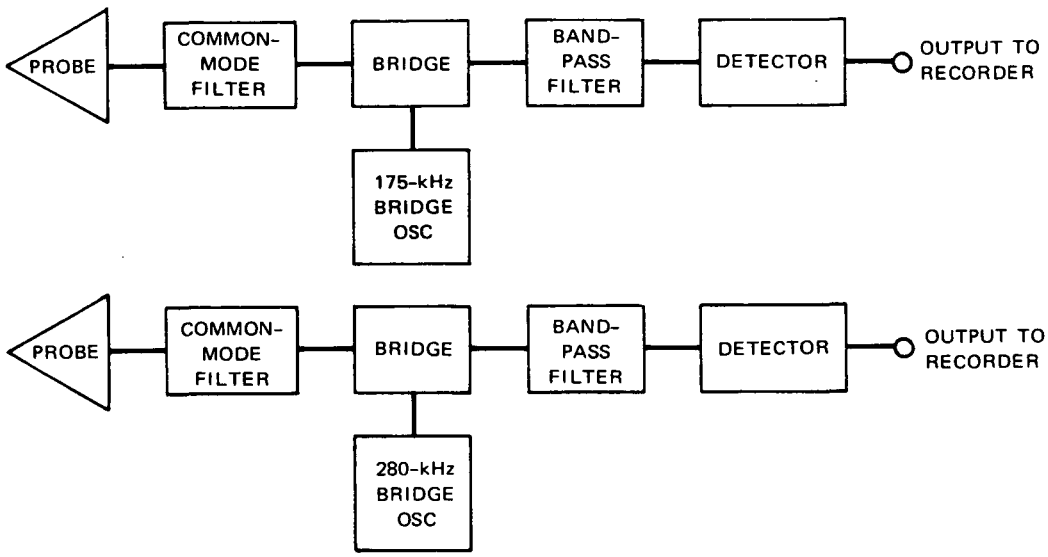

FIGURE 2 BLOCK DIAGRAM OF PROBE ELECTRONICS SYSTEM

probe system (output voltage as a function of depth) is shown in Figure 3. The probe response is seen to be linear over this 10-cm interval. The probe design and two sets of probes and electronics were provided to the NASA Langley Research Center as part of the program. An operating procedure and set of circuit diagrams were provided also.

To verify that meniscus effects are negligible on resistance-type staffs, a test program was undertaken. The depth of the probe in still water was varied sinusoidally by a mechanical oscillator supporting the probe. The frequency of oscillation was varied between 0.1 and 5 Hz and the amplitude was varied up to 8 cm. Although 5 Hz is lower than the highest frequency of interest, Colonell[11] observes that the water surface can be accelerated only as much as the acceleration due to gravity. As a consequence, probe oscillations having a combination of amplitude and frequency giving that limit are sufficient to test the

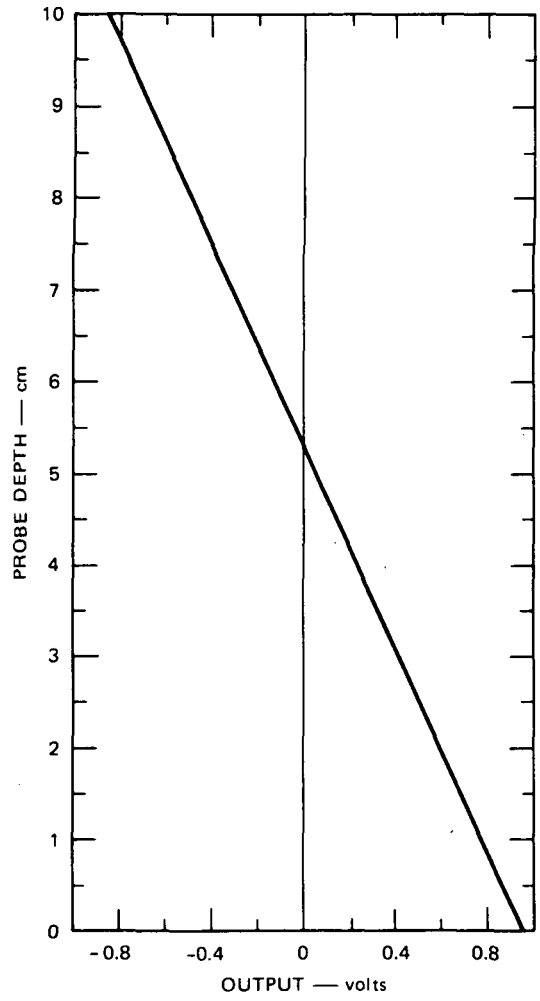

FIGURE 3 SAMPLE CALIBRATION CURVE OF RESISTANCE-TYPE WAVE STAFF

ability of a probe to respond to wave-height changes. In the current tests, accelerations in excess of that of gravity were applied.

Figure 4 shows the probe output as a function of depth for six of the twenty different combinations of amplitude and (mechanical) frequency that were documented in the error study. (Nominally, amplitude increases from bottom to top photos, while frequency increases from left to right photos.) The maximum drainage and meniscus errors, which give hysteresis-type signatures, are expected for the conditions with maximum acceleration (at the ends of the excursions). Indeed, the tests with maximum acceleration near that of gravity [Figs. 4(d) and 4(e)] show the maximum absolute error. In any case, the error is seen not to exceed 1 mm. In fact, for the larger amplitudes, it appears that the error is no greater than the nominal oscilloscope line width. The hysteresis effect seen in Figure 4(c) is a consequence only of "play" in the mechanical drive, while in 4(f) the effects are due to a combination of this and of meniscus drainage.

To examine the effects of the proximity of one staff on the dynamic response of a second, further tests were undertaken. It was determined that the linearity and slope of the probe response to height fluctuations were not perturbed by the presence of a second probe. For purposes of correlation measurements, only the linearity of the probe response to the wave-height fluctuations is important, and therefore these probes are suitable sensors of wave-height statistics.

With the completion of these tests, the suitability of wave staffs for measurement of the wave-height fluctuations has been demonstrated. In the next section, the measurement program in the wind-wave tank will be discussed.

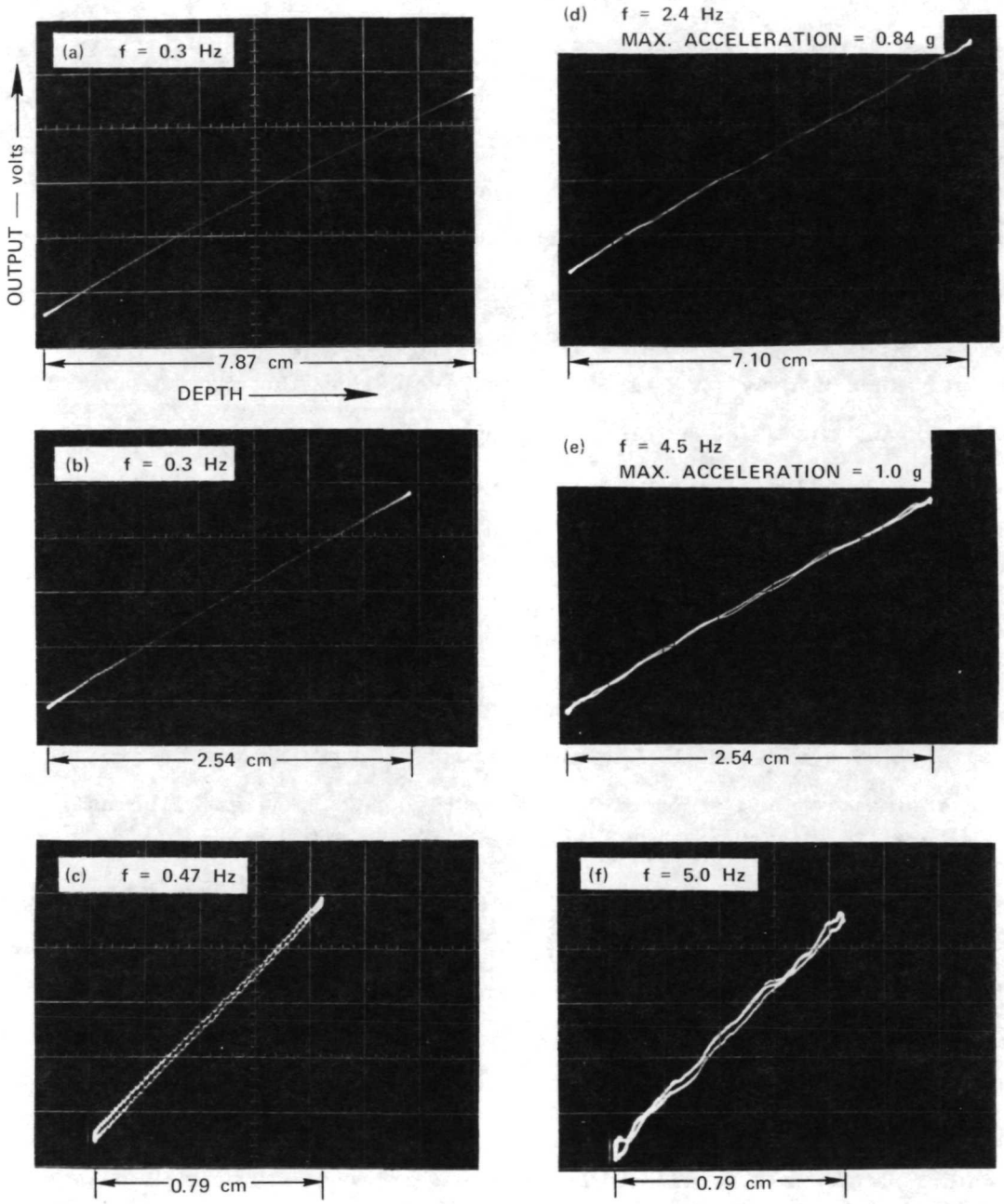

FIGURE 4 RESULTS OF PROBE-ERROR STUDY

III MEASUREMENTS OF WAVE-HEIGHT FLUCTUATIONS

With the development of the wave-height sensors, measurements of the wave-height fluctuations in a wind-wave tank were undertaken. The SRI wind-wave tank is shown schematically in Figure 5. The tank has a cross section 1.83 m (6 ft) by 1.83 m (6 ft) and is 9.1 m (30 ft) in length. It is filled with 0.9 m (3 ft) of water. Two blowers, with a total capacity of 60,000 cubic feet per minute, can blow winds up to 18 m/s ($\approx$ 36 knots) over the surface of the water. Figure 6 shows the wave condition in the wave tank at a wind speed of 16 m/s. The larger figure is looking through the plexiglas wall toward the beach (reflections from the beach are negligible). The inset to this figure gives a closer view of the wave structure. It is seen that there is considerable foam and spray for this wind condition.

A. Data Recording

The output of the wave-staff electronics is recorded on an Ampex FR1300 analog tape recorder with FM electronics. The data are recorded in bursts of 25.6 s. The signal-to-noise capability of this recorder is about 40 dB. The frequency spectrum of the wave-height fluctuations of wind-driven waves is sharply peaked (for example, the 30dB bandwidth of the waves of this experiment is only 25 percent of the dominant frequency). When such a signal is recorded on a tape recorder, the limit on measurable frequency content is the tape-recorder signal-to-noise-ratio specification. To circumvent this constraint, the desired signal can be preconditioned by "whitening" or compensated before it is recorded. To this end, a simple high-pass RC network with a cutoff of 12 dB per octave and a cutoff frequency of 10 Hz was designed and constructed for use in this experiment to permit measurements of the

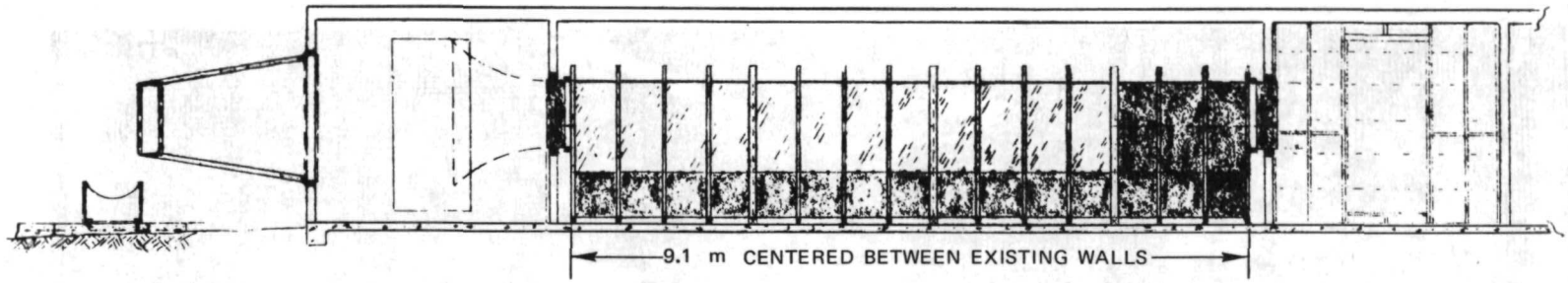

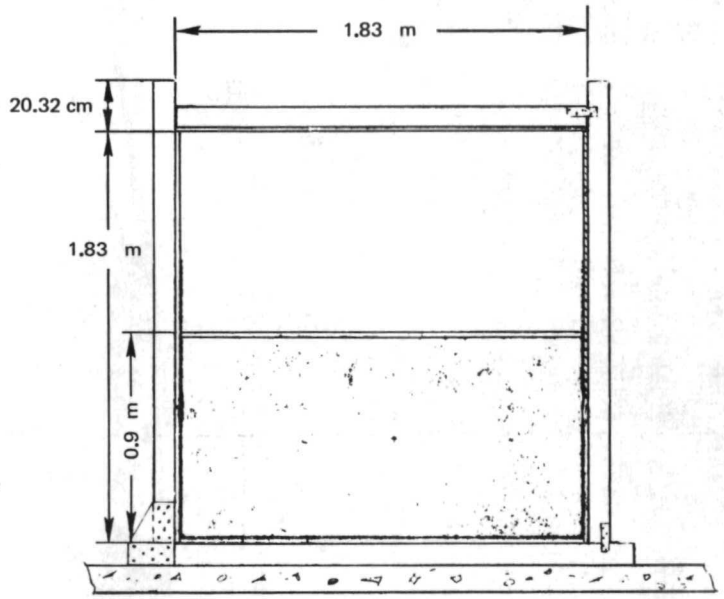

FIGURE 5 WIND-WAVE TANK

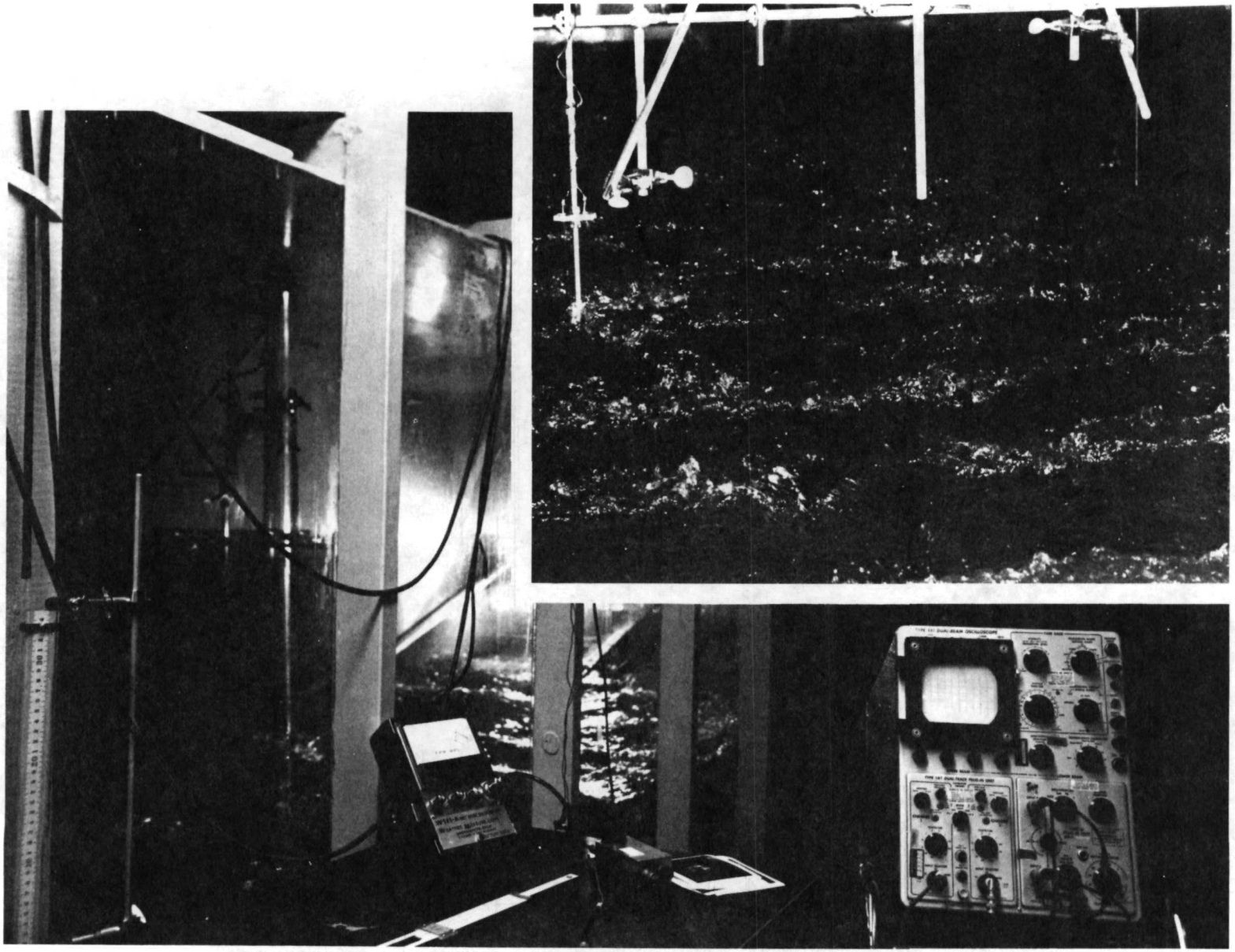

FIGURE 6 WIND-GENERATED WAVES IN THE SRI TANK

frequency spectrum up to 20 Hz. The power response function G(f) of this network is given by:

$$G(f) \approx [1 + (10/f)^2]^{-2} \qquad (2)$$

where f is frequency in Hz. More elaborate compensating networks can easily be constructed.

B. Data Processing

The recorded analog data are A/D converted at a 40-Hz sampling rate. The cross correlation and autocorrelation coefficients and the PSD function of wave-height fluctuations are numerically computed. For the computations, from a pair of probes an ensemble of 20 records of duration T seconds (usually T = 6.4 s or 25.6 s) is averaged. To suppress the sidelobes in the frequency domain, each time record is weighted with the Tchebysheff polynomial.[12] The Tchebysheff weighting function was chosen to suppress the sidelobe level to less than 60 dB below the mainlobe peak.

The complex spectrum of each of the weighted time records is determined using Fast Fourier Transform (FFT) techniques. Define $H_{1i}(f)$ and $H_{2i}(f)$ as the complex spectra of the i^{th} record of the weighted time functions at two points in space separated a distance $\vec{\delta}$. The averaged cross spectrum $H_{12}(f)$ (where the δ dependence has been suppressed) is given by

$$H_{12}(f) = |H_{12}(f)|e^{j\varphi(f)} = \frac{1}{20}\sum_{i=1}^{20} H_{1i}^{*}(f)\, H_{2i}(f)$$

$$= \frac{1}{20}\sum_{i=1}^{20} |H_{1i}(f)|\ |H_{2i}(f)|e^{j(\varphi_{2i}-\varphi_{1i})} \qquad (3)$$

where $|H_{12}(f)|$ is the magnitude of the cross spectrum and $\varphi(f)$ its phase. The Fourier transform of the averaged cross spectrum is the space-time correlation coefficient, $R(\vec{\delta},\tau)$, for the probe separation $\vec{\delta}_p$, defined in Eq. (1b). As $\vec{\delta} \rightarrow 0$, the time records become identical and $R(\vec{\delta},\tau)$ becomes $R(0,\tau)$, the temporal autocorrelation coefficient; and $|H_{12}(f)|^2$ becomes the temporal PSD function of wave-height fluctuations at a point, $|H(f)|^2$. The two-dimensional Fourier transform of $R(\vec{\delta},0)$, measured at sufficient points to adequately define this curve, is the spatial PSD function of the surface fluctuations. For every probe separation, $\vec{\delta}$, the autocorrelation coefficient and PSD function of each probe as well as the cross-correlation coefficient and the phase of the cross spectrum were computed and plotted as shown in Figure 7. The figure shows the aforementioned quantities for a wind speed of 13.0 m/s, a probe separation of 8 cm along the wind vector, and at a fetch (i.e., the length of water surface parallel to the wind direction that experiences wave-generating action of the wind) of 6 m. In the following paragraphs the data taken in the wind-wave tank will be presented.

C. Time-Domain Results

The two-dimensional space-time correlation coefficients were measured at three wind speeds--6, 9, and 13 m/s at a fetch of 6 m. These data are presented in various formats in the following sections.

1. Wind Speed of 6 m/s

Figure 7 shows the measured space-time correlation coefficients at several probe separations along the wind vector. The correlation is observed to peak at a time delay, τ_M, for probe separations, δ. Under the assumption that waves propagate in a narrow cone of angles about the wind vector, the group velocity of the wave packets can be inferred from the data as having the format shown in Figure 8. Figure

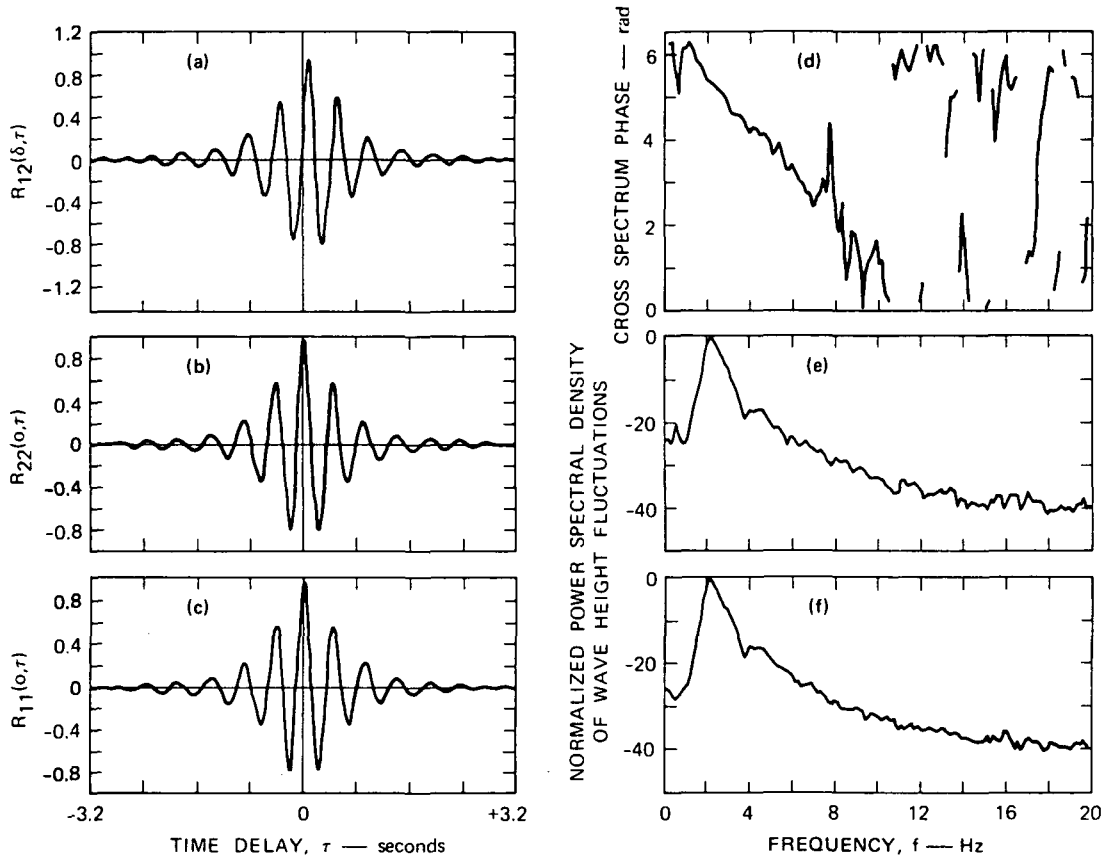

FIGURE 7 WAVE-HEIGHT STATISTICAL-DATA FORMAT

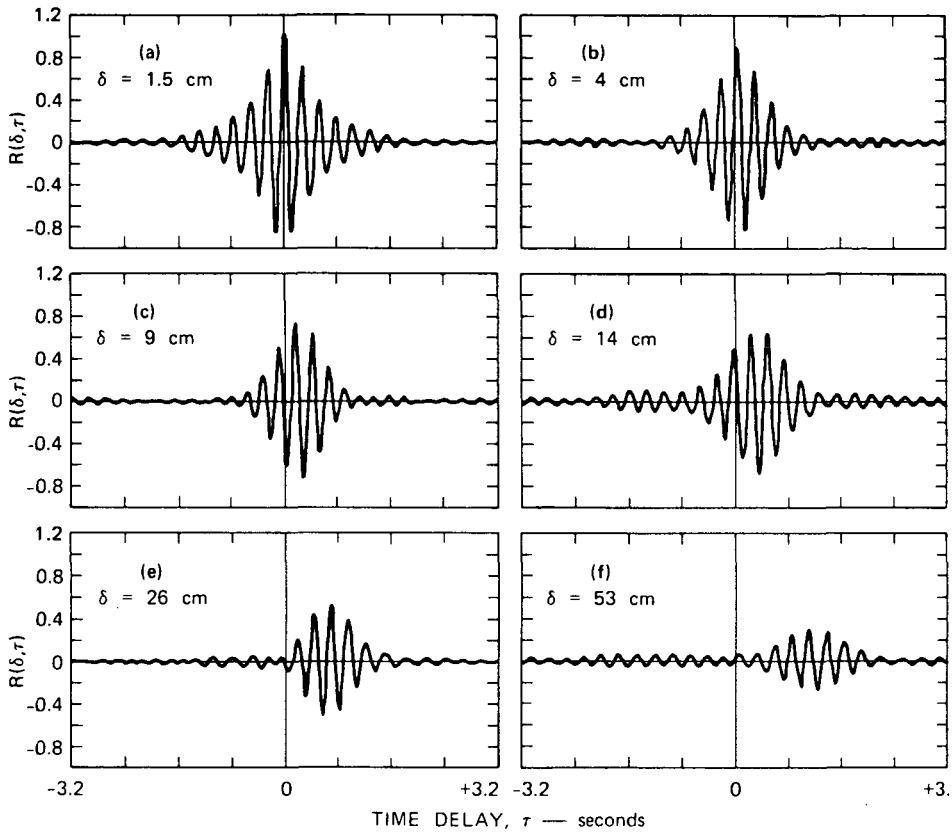

FIGURE 8 SPACE-TIME CORRELATION COEFFICIENT FOR LONGITUDINAL PROBE SEPARATION, δ, AND WIND SPEED = 6 m/s

Figure 9 shows the optimum space-time correlation coefficient, $R(\vec{\delta},\tau_M)$, [i.e., for any probe separation, $R(\vec{\delta},\tau_M)$ is the peak correlation of the envelope of the correlation coefficient] as a function of probe separation. As the probe separation increases, this quantity indicates the degree to which wave propagation is "frozen". For frozen flow (one-dimensional propagation in a non-dispersive medium) $R(\vec{\delta},\tau_M)$ would remain at a value of 1.0 for all probe separations δ. Figure 10 shows some measured space-time correlation coefficients for probe separations transverse to the wind vector. It is seen in these data that the peak correlation occurs for zero time delay, independent of probe separation, for probe separations up to 8 cm.

Figure 11 shows the data points for the measured spatial correlation coefficient along and transverse to the wind vector. The spatial correlation data of this figure are qualitatively similar to those reported by Medwin.[13] Wave-height statistical data were also obtained along radii, at constant angles to the wind vector, for increments in angle of 15°. The symmetry of the correlation coefficients about the wind vector was verified as well. Figure 12 shows the measured spatial correlation coefficient, specified in polar coordinates, for probe separations along radii at constant angle to the wind vector. The angle θ is zero for measurements along the wind vector. In this figure a smooth curve through the data is shown. The data in Figure 12 indicate that the dominant oscillatory motion has the same wavelength if the correlation coefficients are plotted against $\delta_r \cos\theta$. This result is consistent with the idea of one-dimensional wave propagation. The envelope of the spatial correlation coefficient is an estimator of wave packet size. The packets are observed to be anisotropic with a 2-to-1 aspect ratio--i.e., the packet dimension along the wind vector is twice the dimension transverse to the wind vector.

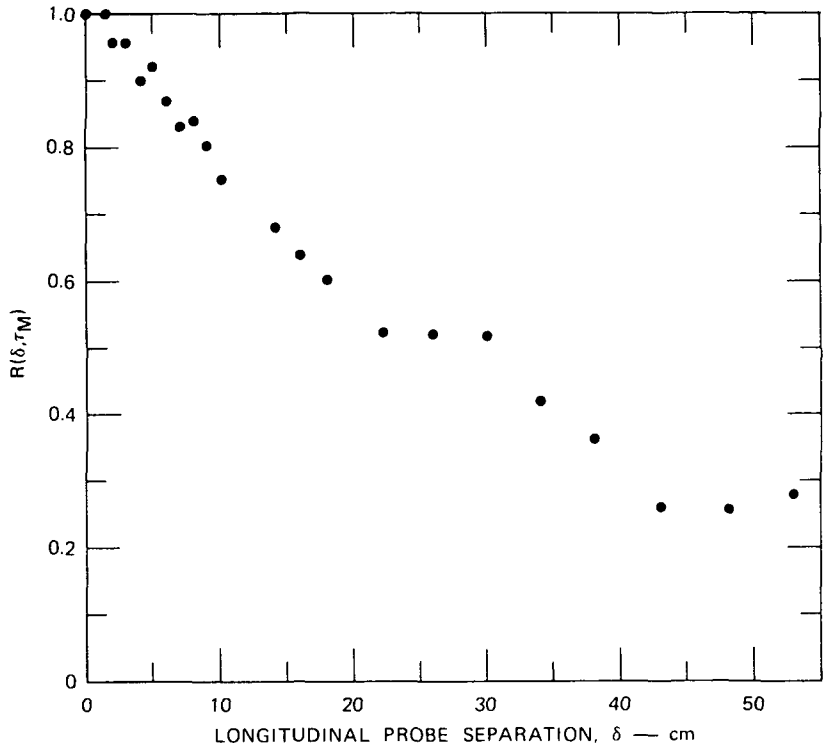

FIGURE 9 OPTIMUM SPACE-TIME CORRELATION COEFFICIENT vs. PROBE SEPARATION — WIND SPEED = 6 m/s

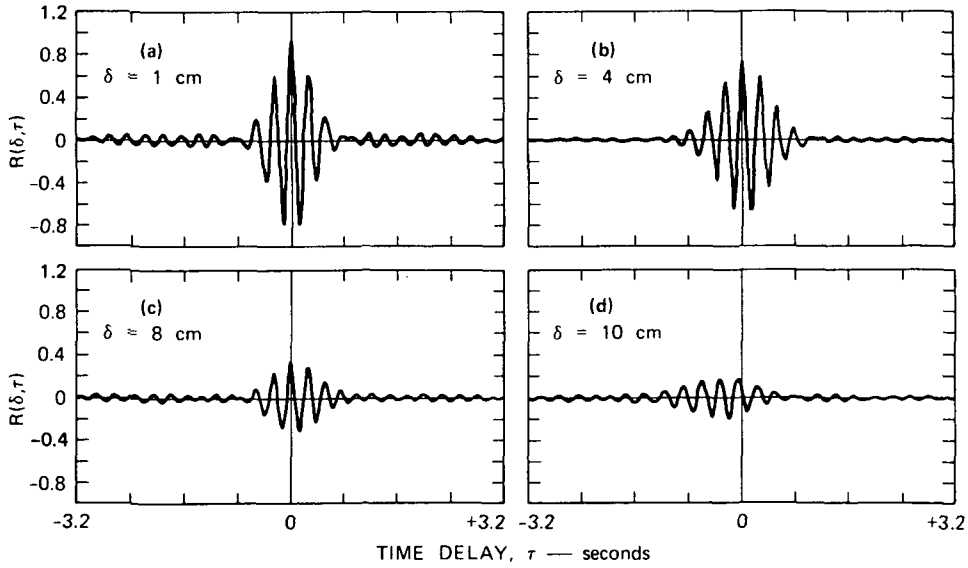

FIGURE 10 SPACE-TIME CORRELATION FOR TRANSVERSE PROBE SEPARATIONS, δ, AND WIND SPEED = 6 m/s

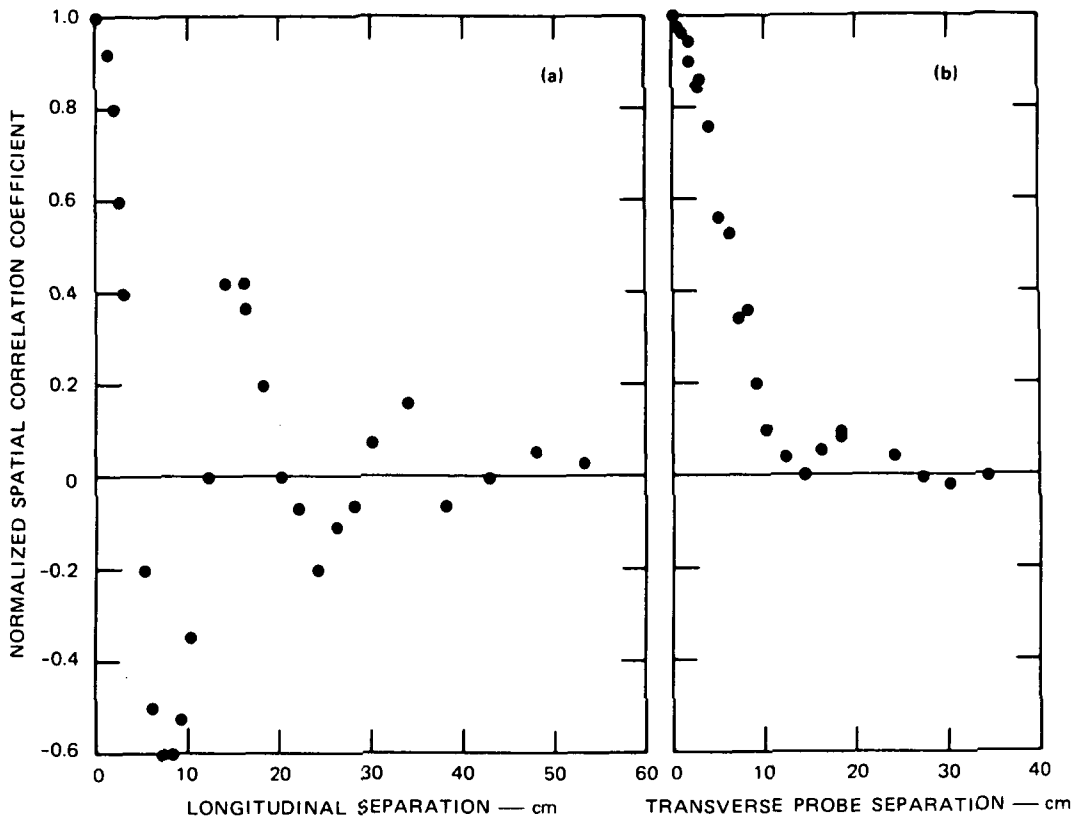

FIGURE 11 NORMALIZED SPATIAL CORRELATION COEFFICIENT (a) ALONG, AND (b) TRANSVERSE TO THE WIND VECTOR. Wind speed = 6 m/s.

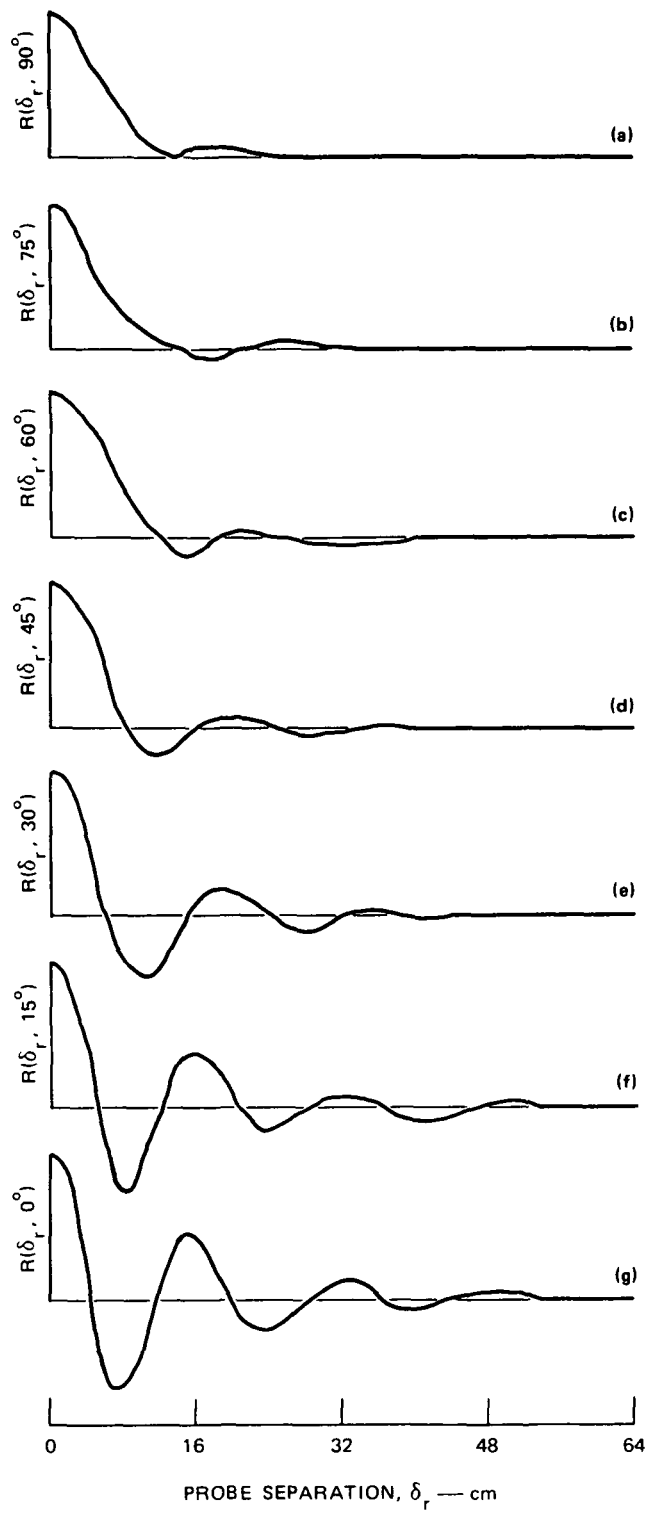

FIGURE 12 NORMALIZED SPATIAL CORRELATION IN 15° INCREMENTS TO THE WIND VECTOR — WIND SPEED = 6 m/s

2. Wind Speed of 9 m/s

Figure 13 shows the measured space-time correlation coefficients at several probe separations along the wind vector. The character of the data is similar to that of the comparable data shown for

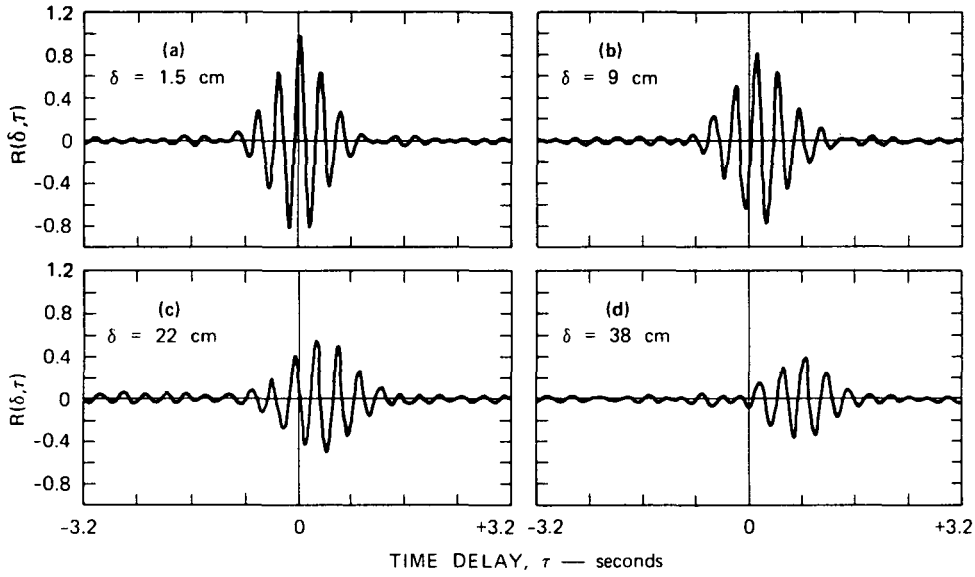

FIGURE 13 SPACE-TIME CORRELATION COEFFICIENT FOR LONGITUDINAL PROBE SEPARATION, δ, AND WIND SPEED = 9 m/s

a wind speed of 6 m/s. Figure 14 shows the optimum space-time correlation coefficient as a function of longitudinal probe separation. Figure 15 shows some representative space-time correlations for transverse probe separations. The spatial correlations for longitudinal and transverse probe separations are illustrated in Figure 16 where it is observed that the wave packets are again anisotropic, with a length to diameter ratio of approximately 2.

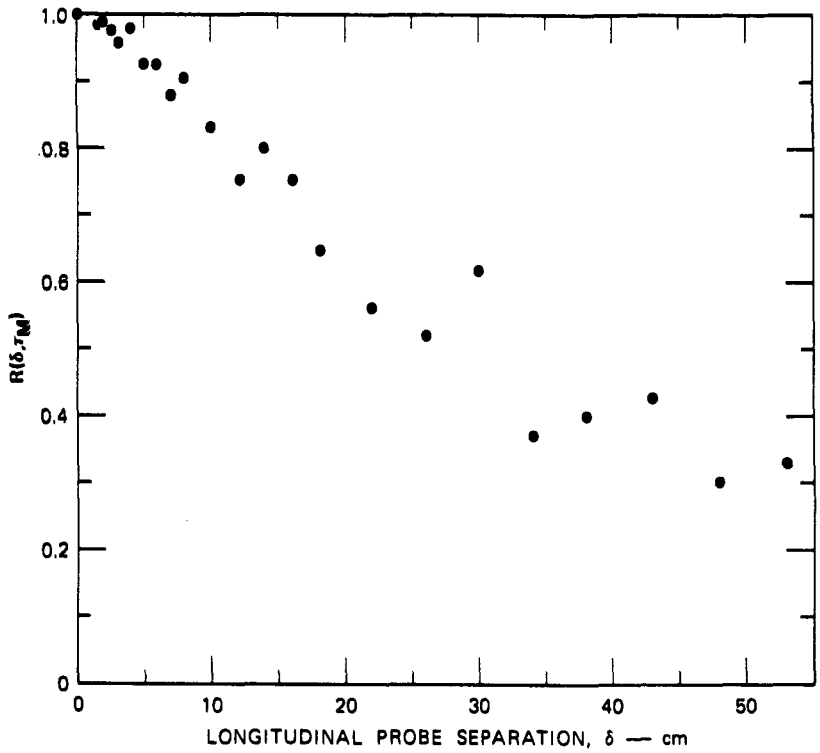

FIGURE 14 OPTIMUM SPACE-TIME CORRELATION COEFFICIENT vs. PROBE SEPARATION, WIND SPEED = 9 m/s

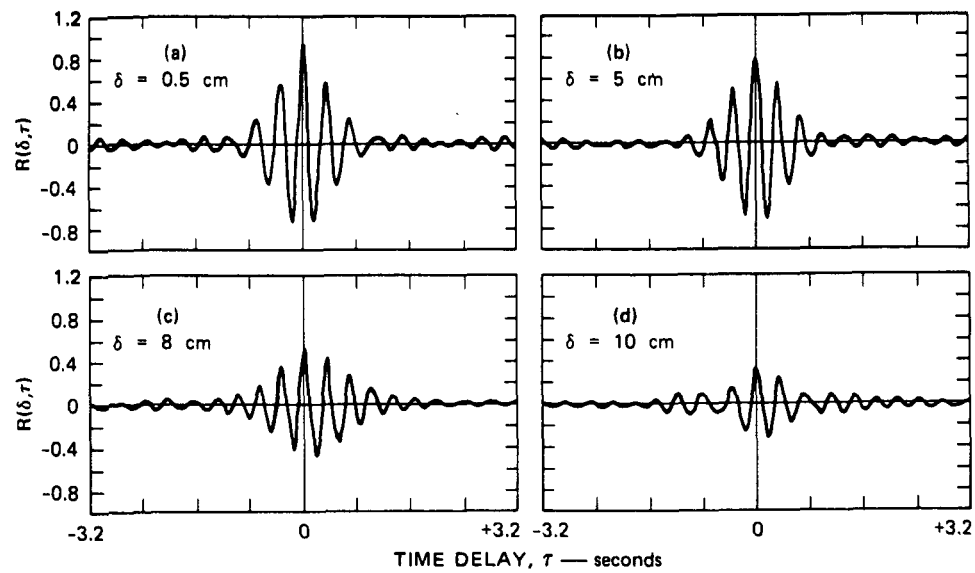

FIGURE 15 SPACE-TIME CORRELATION FOR TRANSVERSE PROBE SEPARATIONS, δ, AND WIND SPEED = 9 m/s

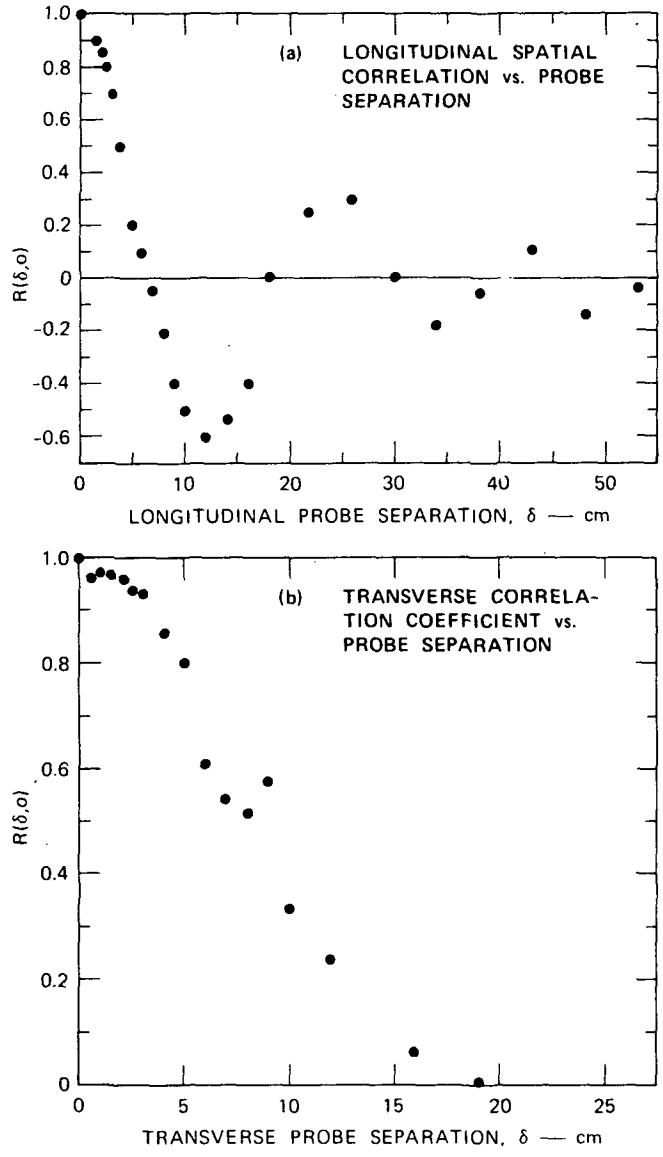

FIGURE 16 NORMALIZED SPATIAL CORRELATION COEFFICIENT (a) ALONG, AND (b) TRANSVERSE TO THE WIND VECTOR. Wind speed = 9 m/s.

3. Wind Speed of 13 m/s

The correlation coefficients similar to those shown previously at 6 and 9 m/s are shown in Figures 17 through 20 for a wind speed of 13 m/s. The data are qualitatively very similar to those shown at lower wind speeds.

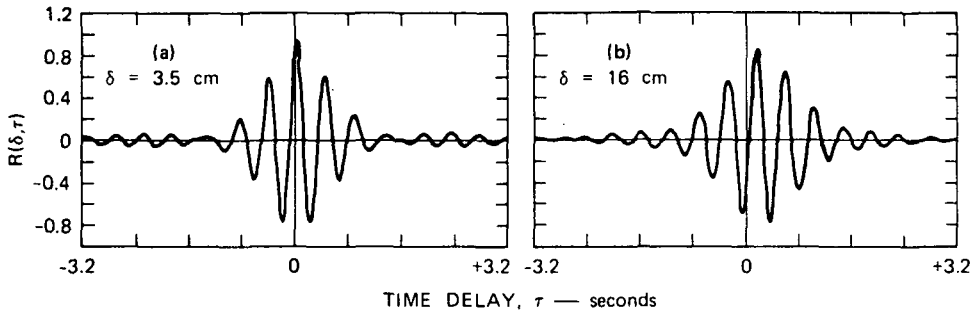

FIGURE 17 SPACE-TIME CORRELATION COEFFICIENT FOR LONGITUDINAL PROBE SEPARATION, δ, AND WIND SPEED = 13.2 m/s

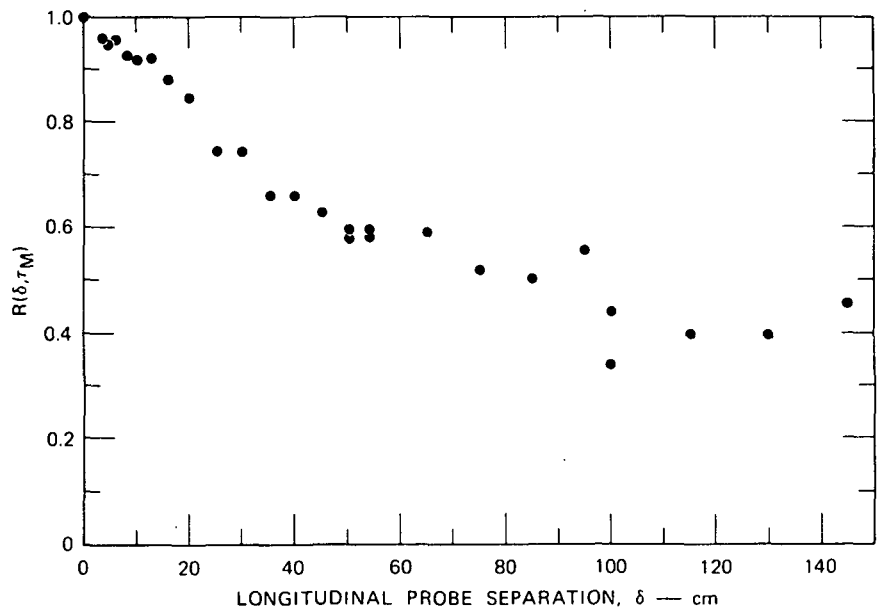

FIGURE 18 OPTIMUM SPACE-TIME CORRELATION COEFFICIENT vs. PROBE SEPARATION — WIND SPEED = 13.2 m/s

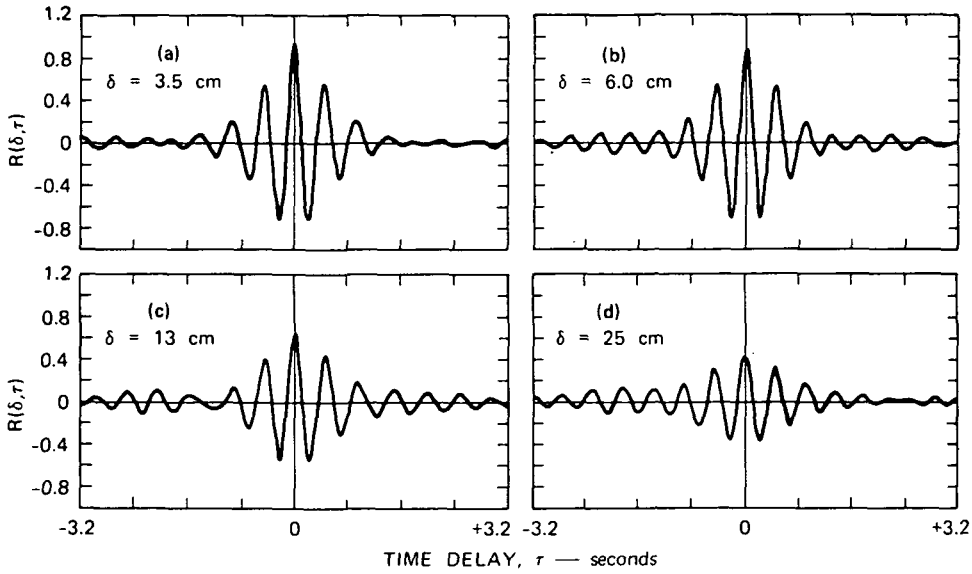

FIGURE 19 SPACE-TIME CORRELATION FOR TRANSVERSE PROBE SEPARATIONS, δ, AND WIND SPEED = 13.2 m/s

D. Frequency-Domain Results

The temporal PSD function of the wave-height fluctuations, $|H(f)|^2$, is the Fourier transform of the autocorrelation coefficient:

$$|H(f)|^2 = \int_{-\infty}^{\infty} R(0,\tau) \exp i(2\pi f\tau)\, d\tau \qquad (3)$$

or

$$|H(f)|^2 = \left| \int_{-\infty}^{\infty} h(t) \exp i(2\pi ft)\, dt \right|^2 \qquad (4)$$

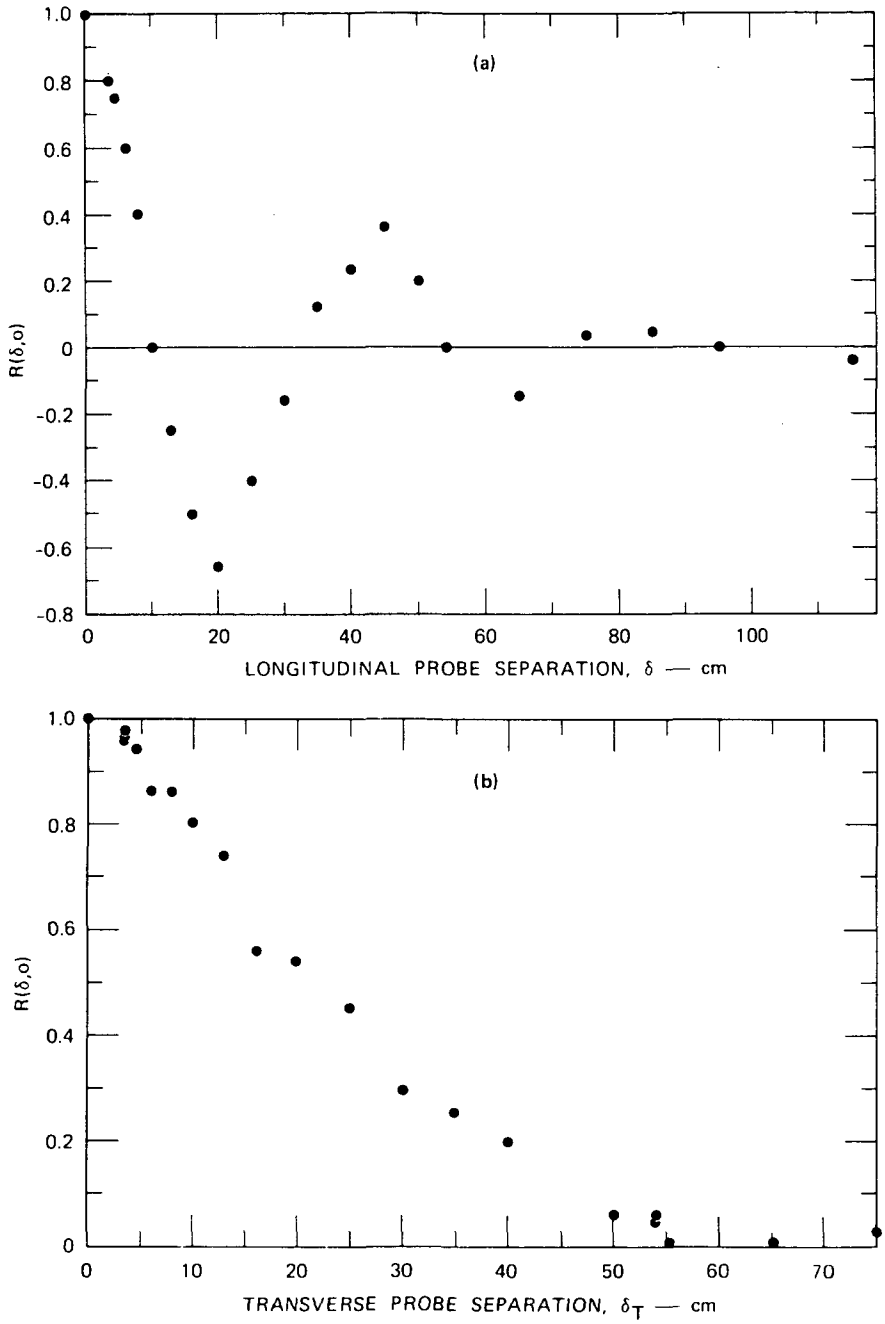

FIGURE 20 NORMALIZED SPATIAL CORRELATION COEFFICIENT (a) ALONG, AND (b) TRANSVERSE TO THE WIND VECTOR. Wind speed = 13.2 m/s.

The temporal PSD function of the wave-height fluctuations measured in the wind-wave tank is plotted in Figure 21 for various wind speeds at a fetch of 6.5 m. There are a number of observations that can be made of these data. A second-harmonic component is observed at all wind speeds (the second-harmonic component at 8 m/s manifests itself as a shoulder to the fundamental component). Tests of the electronic instrumentation associated

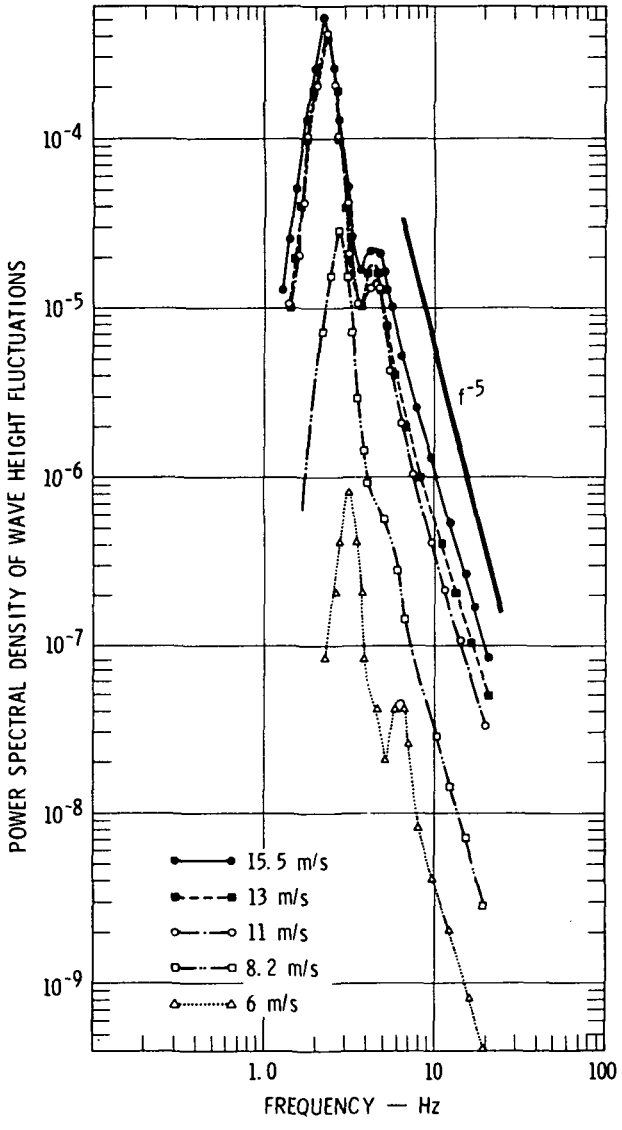

FIGURE 21 POWER SPECTRAL DENSITY FUNCTION OF WAVE-HEIGHT FLUCTUATION FOR SEVERAL WIND SPEEDS AT A FETCH OF 6.5 m

with the wave staffs and the staffs themselves showed that this effect was not due to the measuring system. As a consequence, it is believed that this is indeed a water-wave phenomenon. In the next section, these observations of second-harmonic components will be shown to agree with calculations based upon theory.

It is further observed in Figure 21 that the fundamental components of the wave spectra exhibit a "saturation" effect--i.e., the amplitude at a given frequency component reaches a maximum and does not increase with increasing wind speed. By way of contrast, the components beyond the second-harmonic peak do not saturate. This result is consistent with a second-harmonic theory, as will be discussed in the next section. The high-frequency components are observed to exhibit 5th-power decay with increasing frequency (i.e., $|H(f)|^2 \propto f^{-5}$), as proposed by Phillips.[14]

The temporal PSD function of wave-height fluctuations is plotted in Figure 22 as a function of fetch for a wind speed of 6 m/s. The frequency of the dominant component is seen to decrease with increasing fetch although the wave amplitude grows with fetch. A "saturation" in the amplitude of the frequencies of the fundamental component is evident in this data as well.

The phase velocity and spatial wavelength in a particular direction can be determined by examining the phase difference of the spectral components measured at two points. This phase difference is spoken of as the "phase" of the cross spectrum. Measurements of the phase of the cross spectrum as a function of frequency are shown in Figure 23 for several longitudinal separations of the probes and in Figure 24 for several transverse probe separations at a wind speed of 6 m/s. The phase of the cross spectrum for longitudinal separations is well defined and evidences some dispersion (as discussed in Section IV) for small separations at all frequencies. As the probe separations get larger,

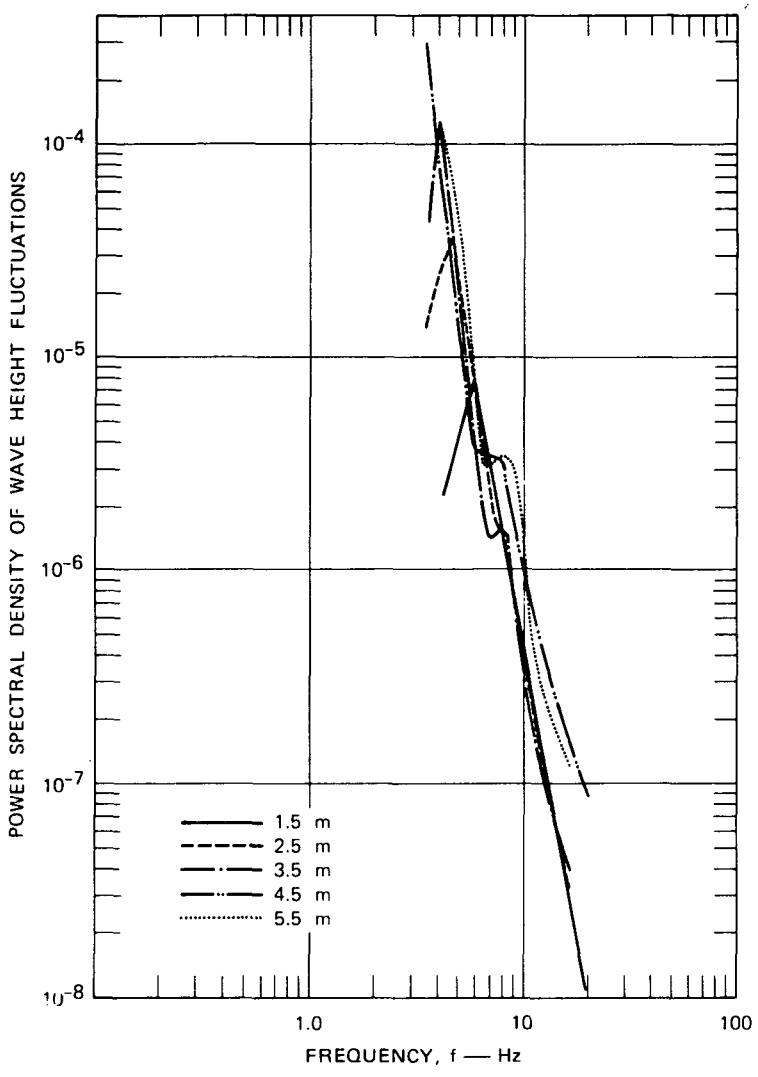

FIGURE 22 POWER SPECTRAL DENSITY FUNCTION OF WAVE-HEIGHT FLUCTUATION AT A WIND SPEED OF 6 m/s FOR VARYING FETCH

the high-frequency components become decorrelated (as evidenced by a uniform probability for the phase to be anywhere between 0 and 2π), but the low frequencies continue to show dispersive effects. A discontinuity in the slope of the phase of the dispersion occurs at frequencies in excess of about 5/3 of the dominant frequency component. This is a manifestation of the second-harmonic-wave components. The relative phase for transverse probe separations remains reasonably constant, indicating no average transverse velocities. (That is, the transverse phase velocity

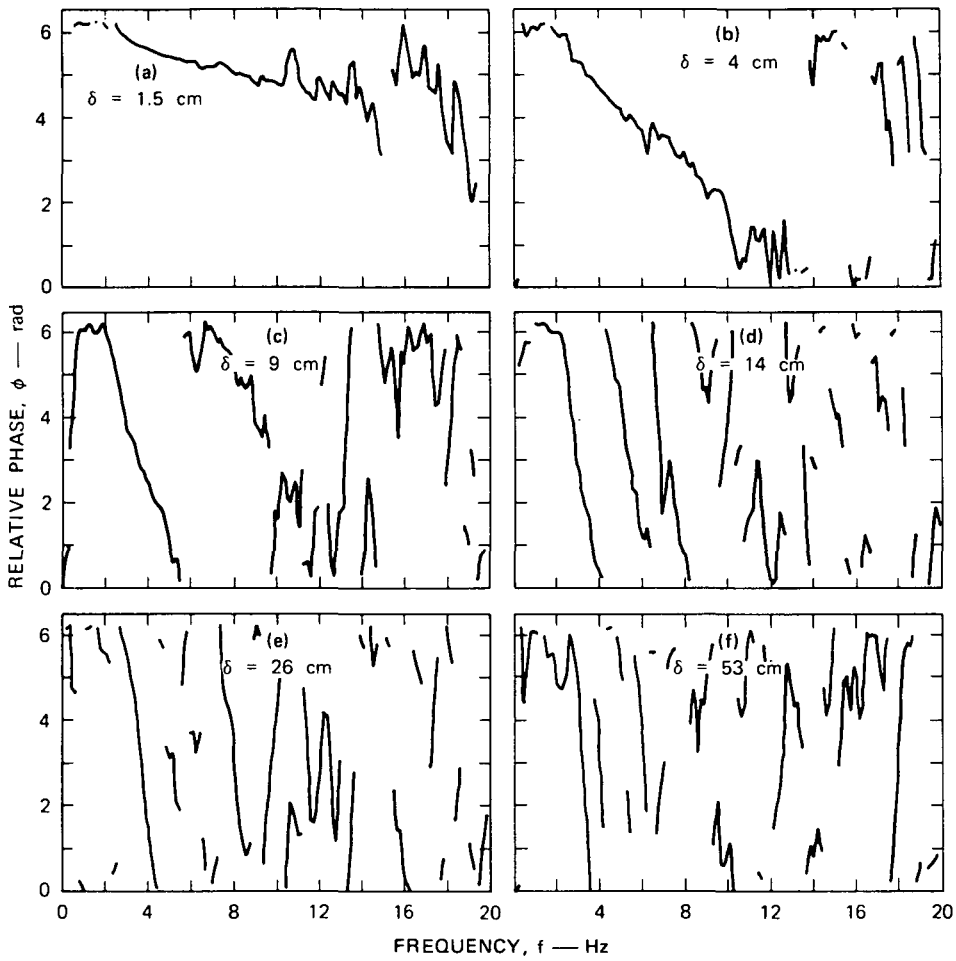

FIGURE 23 MEASURED RELATIVE PHASE ON LONGITUDINALLY SEPARATED PROBES vs. FREQUENCY FOR VARYING PROBE SEPARATIONS — WIND SPEED = 6 m/s

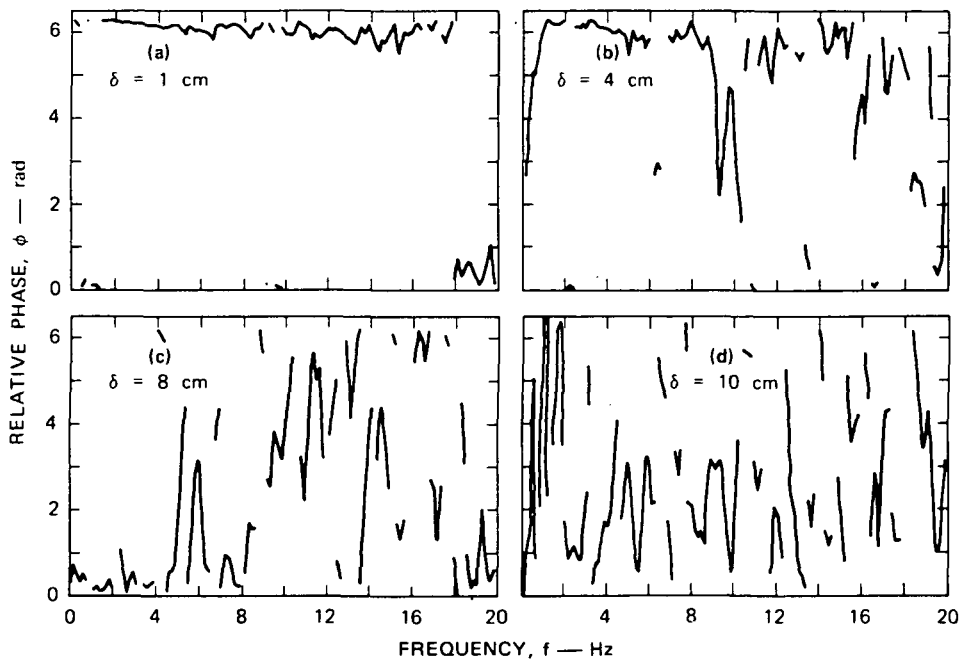

FIGURE 24 MEASURED RELATIVE PHASE ON TRANSVERSELY SEPARATED PROBES vs. FREQUENCY FOR VARYING PROBE SEPARATIONS — WIND SPEED = 6 m/s

is infinite.) For increasing probe separations, the higher-frequency components evidence decorrelation. Figures 25 and 26 show the measured relative phase as a function of frequency for several probe separations and for a wind speed of 9 m/s. The character of these data is similar to that shown for the 6-m/s data.

A variety of data obtained in the wind-wave tank have now been presented. The next section will discuss some implications of the observations.

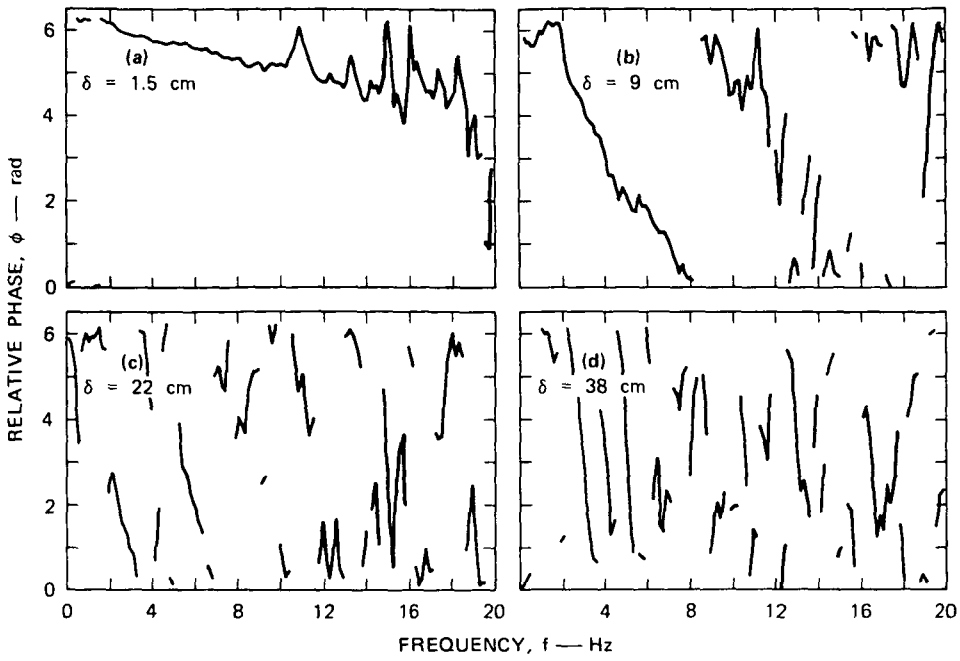

FIGURE 25 MEASURED RELATIVE PHASE ON LONGITUDINALLY SEPARATED PROBES vs. FREQUENCY FOR VARYING PROBE SEPARATIONS — WIND SPEED = 9 m/s

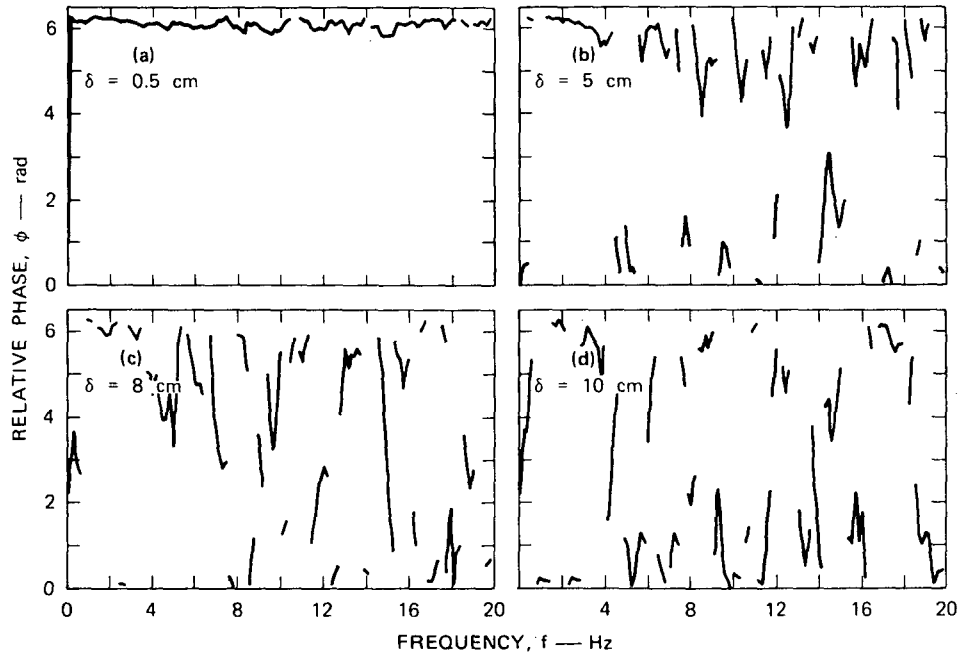

FIGURE 26 MEASURED RELATIVE PHASE ON TRANSVERSELY SEPARATED PROBES vs. FREQUENCY FOR VARYING PROBE SEPARATIONS — WIND SPEED = 9 m/s

IV DISCUSSION OF RESULTS

The measurements shown in the foregoing section can be interpreted unambiguously if the spatial two-dimensional power spectral density (PSD) function of wave-height fluctuations can be calculated. In principle, the PSD function is obtained by taking a straightforward two-dimensional Fourier Transform of the two-dimensional spatial correlation coefficient (in a form such as shown in Figure 12). A calculation of the PSD function was made with the data of Figure 12. The results of the calculation were sufficient to define the dominant wavenumber and a 40-percent bandwidth about the dominant wavenumber. This wavenumber band defined only the first 10 dB of the PSD function. Beyond this bandwidth the PSD function exhibited the effects of statistical error (in the form of negative values of the PSD function). These statistical errors are a consequence of the nonstationarity in the measurements of the two-dimensional correlation coefficient. The measurements of correlation coefficients shown in Figure 12 took one week's test time, since they were made with a single pair of probes having a variable spacing. In the course of this test time, the wind speed, air temperature, etc.(and therefore the wave-height fluctuation statistics) could not be maintained with sufficient accuracy to calculate the PSD function over a greater dynamic range than 10 dB. Greater dynamic range can be achieved by using a wave-staff array (an array of probes) making simultaneous measurements at a number of probe separations.

The measurements in the wind tank lend themselves to a consistent set of results with the assumption that the wave propagation in the wind-wave tank is approximately one-dimensional. This approximation allows us to relate temporal frequency fluctuations to spatial wavenumber

fluctuations in a way that is analogous to the Taylor hypothesis in turbulent fluids.

With the foregoing assumption, the phase of the cross spectrum becomes an indicator of wave dispersion. For transverse probe separation, the phase should not exhibit (and in fact does not exhibit) a finite velocity at any frequency. For longitudinal separation, the phase, $\varphi(f, \delta)$, should vary as

$$\varphi(f, \delta) = \frac{2\pi f \delta}{U_0 + U(f)} \tag{5}$$

where U_0 is the drift current (if any exists) on the surface, and U(f) is the phase speed of the waves and is a well-known function of frequency.[15]

If a drift current exists on the surface, a wave frequency, f, becomes translated to a stationary observer. The apparent frequency, f_a, to a stationary observer of a wave frequency, f, is given by

$$f_a = f \left[\frac{U_0 + U(f)}{U(f)} \right] .$$

When the formalism of Eq. (5) was fitted to the measured longitudinal phase data at 6, 9, and 13 m/s, the agreement between calculation and measurement was very good for frequencies less than about 5/3 times the dominant frequency, and indicated a drift current of 5.4, 7.5, and 18 cm/s, at wind speeds of 6, 9, and 13 m/s, respectively. To test this estimate of drift speed, direct measurements of the surface drift current were made. These measurements were accomplished by timing particles introduced into the water as they passed two stations at a fixed distance apart in the tank. It was found that care had to be taken that the particles had a negligible amount of area exposed to surface

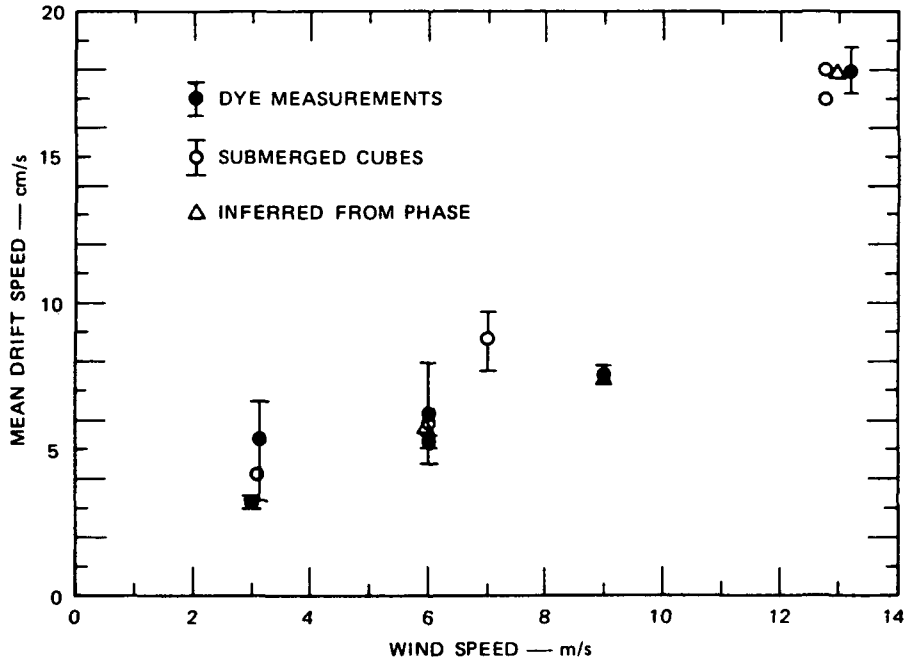

FIGURE 27 MEASURED DRIFT SPEED AS A FUNCTION OF WIND SPEED AT A FETCH OF 6 m

winds. If such a precaution was not observed, erroneous observations resulted. Food dye was also used in place of particles. The food dye was also introduced at the surface. The results of both sets of measurements are shown in Figure 27. A comparison of the drift speeds inferred from phase measurements, as given above, with the direct measurements of drift speed is shown in Figure 27. The agreement is very satisfactory between the two estimates. As previously noted, the phase of the cross spectrum agreed with theory, when drift velocity was taken into account up to about 5/3 the dominant frequency. The agreement between calculation and measurement can be extended to all frequencies if the second-harmonic components are adequately taken into account. Tick[16] has modeled the second-order effect. Essentially, the second-harmonic terms predicted by Tick are coupled to the fundamental terms so that they move at a velocity associated with the fundamental terms. This perturbs the

observed phase. Tick's results can be approximated for the complex second-order frequency spectrum, $H_s(f)$, by

$$H_s(f) \approx \frac{4\pi^2}{g} \int_{-\infty}^{\infty} f'^2 H_F(f') H_F(f-f') \exp\left[\frac{i2\pi f \delta}{U_0+U(f)}\right] \exp\left[\frac{i2\pi(f-f')\delta}{U_0+U(f-f')}\right] df' \quad (6)$$

for frequency, f, beyond the dominant frequency component, f_0, and where g is acceleration due to gravity and the subscripts F and s designate first-order and second-order terms. Equation (6) represents the second-order contribution to the spectrum at a point. The total spectrum is then the sum of the first- and second-order terms. To make a calculation of second-order effects for comparison with measured data, an estimate of the first-order spectrum is required. The signal measured on wave staffs already represents the sum of first- and second-order terms. As a consequence, the definition of the first-order term is ambiguous and some experimentation is required. As an initial estimate, the first-order spectrum $H_F(f)$ was taken to be the measured spectrum $H_M(f)$ except for a band of frequencies ($\sim \pm$ 25 percent) around the second harmonic. In the second-harmonic band the first-order spectrum was taken to be a power-law continuation to the first-order spectrum. That is:

$$H_F(f) \approx H_M(f) \quad , \quad \text{for} \quad f \leq 1.5\, f_0,\ f \geq 2.5\, f_0$$

$$\approx H_M(1.5\, f_0)\ [f/1.5f_0]^{-N}, \quad \text{for } 1.5f_0 \leq f \leq 2.5f_0 \quad (7)$$

where N is chosen so that $H_M(1.5\, f_0)\ [2.5\, f_0/1.5\, f_0]^{-N} \equiv H_M(2.5\, f_0)$.

To calculate the total phase and amplitide characteristic between a pair of probes spaced δ cm apart, an ensemble of 20 data records each of 6.4 s duration was used. The procedure for calculating the complex

cross spectrum was to take the data of an upstream probe, compute the amplitude and phase of the downstream probe, and ensemble-average the product of the upstream probe record with the computed downstream probe record. For each record of the upstream probe a first-order and second-order term is calculated using Eq. (7) and Eq. (6) for zero separation ($\delta = 0$). The spectrum of the upstream probe is then the sum of these terms. For the i^{th} record of the ensemble, this becomes

$$H_1(f) = H_{1iF}(f) + \frac{4\pi^2}{g} \int_{-\infty}^{\infty} f'^2 H_{1iF}(f') H_{1iF}(f-f') \, df' \quad . \tag{8}$$

To calculate the response of a probe downstream of the first probe, the upstream probe record is used. For probe separation δ it should be observed that the first-order term is advanced in phase $\left[2\pi f \delta/[U_0+U(f)]\right]$, so that the downstream probe spectrum of the i^{th} record, $H_{2i}(f)$, becomes

$$H_{2i}(f) = H_{1iF}(f) \exp i\left[\frac{2\pi f \delta}{U_0+U(f)}\right] + \frac{4\pi^2}{g} \int_{-\infty}^{\infty} f'^2 H_{1iF}(f) H_{1iF}(f-f')$$

$$\exp i\left[\frac{2\pi f' \delta}{U_C+U(f')}\right] \exp i\left[\frac{2\pi(f-f')\delta}{U_0+U(f-f')}\right] df' \quad . \tag{9}$$

The twenty records of the ensemble are then averaged as indicated in Eq. (2), and the phase and amplitude of the cross spectrum are predicted. The predicted amplitude and phase are then compared to the measured quantities. For the assumption of the first-order spectrum of the form given in Eq. (7), the agreement is poor. As a second estimator of the first-order spectrum, the functional form was chosen as follows:

$$H_F(f) = H_M(f) \qquad , f \leq (5/3)f_0$$

$$= H_M(5/3\ f_0)\left[f/_{(5/3)f_0}\right]^{-N} , f \geq (5/3)f_0 \tag{10}$$

where N is a variable parameter. With this form as a starting point, the computation was run again and the agreement between calculation and experiment was very good. Figure 28 shows the calculated and measured cross spectrum for a wind speed of 13 m/s, a probe separation of 8 cm, a drift current of 18 cm/s, and N taken equal to 3.5. The agreement between the calculated and measured phase [Fig. 28(b)] is particularly good at frequencies less than 12 Hz. Beyond this frequency, the measured data manifest the effects of decorrelation and some aliasing which were not included in this calculation. The calculated and measured amplitudes agree to within 3 dB for frequencies not affected by aliasing. (Less than about 16 Hz.)

It is of interest to consider the consequences of the second-order effects. From Figure 28(b), it is deduced that the wave dispersion is almost negligible beyond the dominant frequency component (the phase-frequency characteristic is nearly linear, and passes through 0 or 2π for f = 0). This is not surprising when it is recognized that this result implies that the higher order components will propagate at the wave speed of the dominant frequency component, thereby resulting in the maintenance of the non-sinusoidal wave shape as the wave propagates. The observation of increasing amplitude of the second-harmonic components with increasing wind speed (deduced from the results depicted in Figure 21) is also consistent with the second-order effects calculated above. The amplitude of the second-harmonic component will increase with the amplitude of the fundamental component (even though any single frequency in the fundamental component saturates); this is a consequence of the convolution in frequency space.

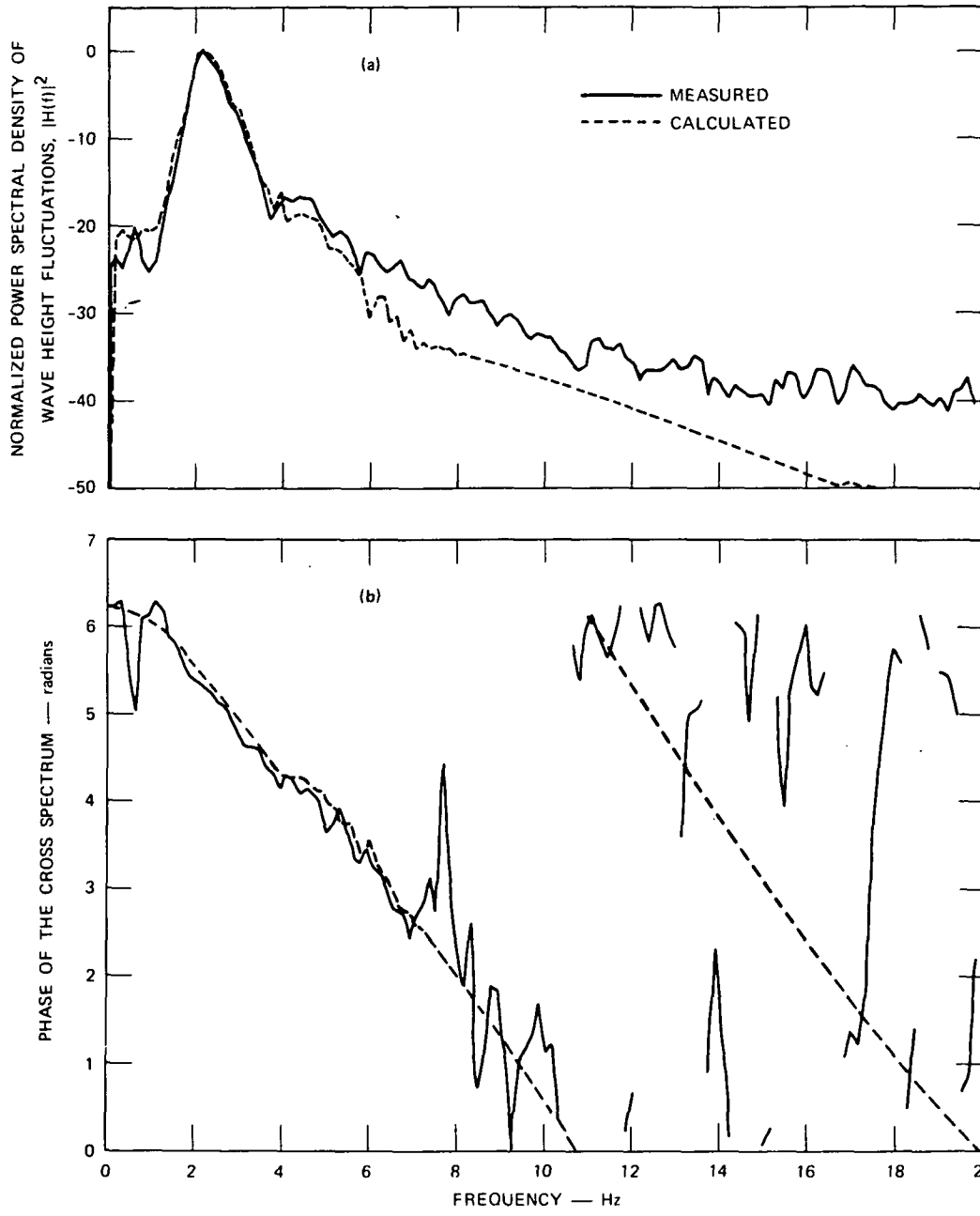

FIGURE 28 COMPARISON OF THE CALCULATED AND MEASURED CROSS SPECTRUM AS A FUNCTION OF FREQUENCY — WIND SPEED = 13 m/s, PROBE SEPARATION = 8 cm, DRIFT SPEED = 18 cm/s

A final test of the assumption of one-dimensional wave propagation is to compute the group velocity of the wave packet and compare the result with an estimate of the group velocity inferred from the space-time correlation measurements. After Fisher and Davies,[17] the group velocity is estimated from the family of space-time correlation coefficients. For all probe separations, the space-time correlation coefficient is plotted. An envelope for this family of curves is then constructed. The point of tangency of the correlation coefficient defines a data point for a δ-t diagram--i.e., for every probe separation there is a time delay for tangency to the envelope. The family of correlation coefficients then defines a line on the δ-t diagram. The slope of this line is the group velocity of the wave packet.

An alternative estimate of group velocity can be obtained since the dispersion relation is known. For a short-gravity-wave packet, the group velocity is

$$V = U(k) + k \frac{dU(k)}{dk} = \frac{U(k)}{2} + U_0 \qquad (11)$$

where U(k) is the phase velocity expressed as a function of wavenumber and U_0 is again the surface drift current. A comparison of the measured and calculated group velocity (with the assumption of one-dimensional wave propagation and using the previously inferred values of drift speed) yields agreement to better than 10 percent for the two estimates for wind speeds of 6, 9, and 13 m/s.

V CONCLUSION AND RECOMMENDATIONS

A resistance-type wave staff has been developed to measure the statistics of wave-height fluctuations. In addition to providing NASA Langley with sets of instrumentation, an initial set of measurements has been conducted in a wave-tank. The temporal PSD function of wave-height fluctuations evidenced second-harmonic components and the spectral variation beyond the second harmonic has a (-5) power-law decay.

The two-dimensional spatial correlation coefficient was measured directly. The longitudinal dimension of the wave packet was twice the transverse dimension. The two-dimensional spatial power spectral density function was computed from the correlation data. The dynamic range of the resulting PSD function was limited, by the nonstationarity of the wave statistics in the time required to perform the experiment (about a week), to 10 dB and a bandwidth of 40 percent around the dominant wavenumber.

With the assumption that the propagation of the waves in the tank was approximatly one-dimensional, the wave-height statistical measurements were used to infer surface drift speeds, and to verify, with very satisfactory results, Tick's second-order perturbation theory for waves.

The initial measurements of wave statistics are very encouraging, but additional effort would be appropriate. A more careful measurement of the two-dimensional correlation coefficient (with an array of probes) to circumvent the difficulties of nonstationarity should be attempted. The validity of the assumption of nearly one-dimensional wave propagation could then be unambiguously determined.

REFERENCES

1. W.J. Pierson and R.K. Moore, "Surface Weather and Wave Conditions" Paper presented at the Ocean World (1970).

2. D.E. Kaufman, "A Vector Solution for Electromagnetic Wave Scattering from a Rough Surface of Arbitrary Dielectric Constant," Radio Science, Vol. 6, p. 7 (1971).

3. W.J. Pierson, F.C. Jackson, R.A. Stacey, and E. Mehr, "Research on the Problem of the Radar Return from a Wind Roughened Sea," paper presented at Advanced Application Flight Experiments Principal Investigator's Review held at NASA Langley Research Center, October 5, 1971.

4. A.H. Schooley, "A Simple Optical Method for Measuring the Statistical Distribution of Water Surface Slopes," J. Opt. Soc. Am. Vol. 44, p. 37 (1954).

5. C.Cox and W. Munk, "Measurement of the Roughness of the Sea Surface from Photographs of the Sun's Glitter," J. Opt. Soc. Am. Vol, 44, p. 838, (1954).

6. J. Wu, J.M. Lawrence, E.S. Tebay, and M.D. Tulin, "A Multiple Purpose Optical Instrument for Studies of Short Steep Water Waves," Rev. Sci. Instr. Vol. 40, p 1209, (1969).

7. D. Stilwell, Jr. "Directional Energy Spectra from Photographs," J. Geophys. Res. Vol. 74, p. 1974 (1969).

8. W.S. Olsen and R.M. Adams, "A Laser Profilometer," J. Geophys. Res. Vol. 75, p. 2185, (1970).

9. C. Cox, "Measurements of Slopes of High-Frequency Wind Waves," J. Marine Res. Vol. 16, p. 199 (1958).

10. W.F. Baker, "A Directional Wavebuoy Operating up to 15 Hertz," paper presented at Conference on Electronic Engineering in Ocean Technology, University College of Swansea, England, 21 to 24 September, 1970.

11. J.M. Colonell, "Laboratory Simulation of Sea Waves," Technical Report No. 65, ONR, Contract Nonr 225(71), NR-62-320, Stanford University, Stanford California (July 1966).

12. K.A. Graf, H. Guthart, and D.G. Douglas, "Processing Wake Data with Deconvolution and Reconvolution Calculations," Scientific Report 1, SRI Project 8197, Contract DAHC60-70-C-0016, Stanford Research Institute, Menlo Park, California (October 1969).

13. H. Medwin and S. Clay, "Dependence of Spatial and Temporal Correlation of Forward Scattered Underwater Sound on the Surface Statistics -- II Experiment," J. Acoust. Soc. Am. Vol. 47, p. 1419, (1970).

14. O.M. Phillips, The Dynamics of the Upper Ocean (Cambridge University Press, Cambridge, Mass., 1966).

15. G. Neumann and W.J. Pierson, "Principles of Physical Oceanography" (Prentice-Hall, Inc., Englewood Cliffs, N.J., 1966).

16. L.J. Tick, "A Nonlinear Random Model of Gravity Waves I," J. Math. and Mech. Vol. 8, p. 643 (1959).

17. M.J. Fisher and P.O.A.L. Davies, "Correlation Measurements in a Non-Frozen Pattern of Turbulence," J. Fluid Mech. Vol. 18, p. 97. (1963).

NASA-Langley, 1972 —— 12 CR-2153

"The aeronautical and space activities of the United States shall be conducted so as to contribute . . . to the expansion of human knowledge of phenomena in the atmosphere and space. The Administration shall provide for the widest practicable and appropriate dissemination of information concerning its activities and the results thereof."

—NATIONAL AERONAUTICS AND SPACE ACT OF 1958

NASA SCIENTIFIC AND TECHNICAL PUBLICATIONS

TECHNICAL REPORTS: Scientific and technical information considered important, complete, and a lasting contribution to existing knowledge.

TECHNICAL NOTES: Information less broad in scope but nevertheless of importance as a contribution to existing knowledge.

TECHNICAL MEMORANDUMS: Information receiving limited distribution because of preliminary data, security classification, or other reasons.

CONTRACTOR REPORTS: Scientific and technical information generated under a NASA contract or grant and considered an important contribution to existing knowledge.

TECHNICAL TRANSLATIONS: Information published in a foreign language considered to merit NASA distribution in English.

SPECIAL PUBLICATIONS: Information derived from or of value to NASA activities. Publications include conference proceedings, monographs, data compilations, handbooks, sourcebooks, and special bibliographies.

TECHNOLOGY UTILIZATION PUBLICATIONS: Information on technology used by NASA that may be of particular interest in commercial and other non-aerospace applications. Publications include Tech Briefs, Technology Utilization Reports and Technology Surveys.

Details on the availability of these publications may be obtained from:

SCIENTIFIC AND TECHNICAL INFORMATION OFFICE

NATIONAL AERONAUTICS AND SPACE ADMINISTRATION

Washington, D.C. 20546